Research Square

Preprints are preliminary reports that have not undergone peer review.
They should not be considered conclusive, used to inform clinical practice,
or referenced by the media as validated information.

Tribological interaction of plasma functionalized $CaCO_3$ nanoparticles with zinc and ashless dithiophosphate additives

Kimaya P Vyavhare
The University of Texas at Arlington
Richard B. Timmons
The University of Texas at Arlington
Ali Erdemir
Texas A&M University College Station
Pranesh B. Aswath (aswath@uta.edu)
University of Texas at Arlington https://orcid.org/0000-0003-2885-1918

Research Article

Keywords: PECVD, CaCO3 nanoparticles, ZDDP, Ashless anti-wear additives, wear, friction, XANES

Posted Date: February 11th, 2021

DOI: https://doi.org/10.21203/rs.3.rs-210447/v1

License: This work is licensed under a Creative Commons Attribution 4.0 International License.
Read Full License

Version of Record: A version of this preprint was published at Tribology Letters on April 5th, 2021. See the published version at https://doi.org/10.1007/s11249-021-01423-z.

Abstract

Surface-modified $CaCO_3$ nanoparticles, synthesized through plasma-enhanced chemical vapor deposition (PECVD), were employed to improve lubricant additive technology for internal combustion engines via reduction and/or replacement of additives, such as zinc dialkyl dithiophosphate (ZDDP), in engine oil. Various oil formulations were prepared with functionalized $CaCO_3$ nanoparticles, in combination with ashless dialkyl dithiophosphate (DDP) and ZDDP at low concentrations of phosphorus. Tribological test results indicate synergistic interaction of functionalized $CaCO_3$ nanoparticles with ZDDP and DDP, providing enhanced friction and wear performance under boundary lubrication. A comparative study of the tribo-surfaces morphology and chemistry was assessed via atomic force microscopy and X-ray absorption near-edge spectroscopy. Improved wear protection by functionalized $CaCO_3$BM (borate and methacrylate coated) nanoparticles under boundary lubrication was attributed to the formation of calcium and boron-rich 50–80 nm thick tribofilms on the worn surfaces. XANES results revealed that plasma functionalized $CaCO_3$ nanoparticles interact with ZDDP and DDP and participate in tribofilm formation through tribo-chemical reactions and metal cation supply to form stable and wear-resistant tribofilms. These results provide strong support for the potential application of plasma functionalized $CaCO_3$ nano-additives to reduce the concentration of harmful P-based additives in automotive lubricants.

1. Introduction

Lubrication in mechanical devices, such as engines, includes continuous improvements to the oils employed to reduce emissions, increase durability, and reduce frictional losses while simultaneously improving overall energy efficiency [1–6]. Lubrication at sliding/rolling contacts in the engine is an interfacial phenomenon with three regimes: boundary, mixed, and hydrodynamic lubrication, wherein the latter provides lower friction and wear. Maximum friction and wear losses occur at the boundary and mixed lubrication regimes in engines, such as the top-ring-reversal region of the piston ring-cylinder liner interface, rolling-sliding contact at cam-follower surfaces, and sliding surfaces in the valve train [7]. Anti-wear additives play a crucial role in reducing wear and preventing the failure of boundary or mixed lubricated interfaces experiencing direct surface asperity collisions due to inadequate lubricant load support. In particular, anti-wear additives are of prime importance in the low viscosity oil currently used in modern engines to substantially reduce viscous energy loss in the engine. Developing more effective automotive lubrication, in combination with lower viscosity base stock and higher-performance, represents an effective route to improve engine efficiency and durability.

Anti-wear additives protect surfaces in relative motion from damage by undergoing mechanochemical dissociation via the formation of surface bond tribofilms. The ability of tribofilms to protect sliding contacts depends, in large part, on their intrinsic properties and their adhesion to the substrate. For example, zinc dialkyl dithiophosphate (ZDDP) is the additive used in current commercial automotive lubricants because of its ability to help form effective tribofilms, and thus act as a sacrificial layer to protect the underlying metal surface [8]. ZDDP tribofilms are well known to form on steel-steel sheared

contacts as a result of stress-assisted, thermally activated chemical reactions [9–11]. To date, extensive research work has been conducted to elucidate the properties and tribofilm forming mechanism involving ZDDP. For example, several studies have shown that effective tribofilms are formed only at high temperatures while, in contrast, at room temperature only weakly bounded tribofilms, and in some cases, no tribofilms, are observed [12, 13]. ZDDP tribofilms exhibit patchy morphology and lower elastic modulus and hardness than that engine components (like steel), which allows them to sacrifice or distribute applied stresses under mild friction at the sliding interface to prevent wear [14]. However, despite being a cost-effective multipurpose additive, their application in engine oil is increasingly questioned due to their several disadvantages. These disadvantages include poisoning of exhaust by thiophosphate byproducts, inadequate wear protection in ultralow viscous lubricants, and micro-pitting in thin-film lubrication [14]. These disadvantages illustrate the need to eliminate, or partially replace, ZDDP in the oil. In recognition of these undesirable side effects, engine oil specifications, introduced between 1994 to 2020, reduced the permitted maximum concentration of phosphorus and sulfur in the engine oil [15]. As a result, current engine oil specifications allow phosphorus level up to only 0.08 wt.%. However, there is a strong possibility that in the future permissible phosphorus content in an engine oil might be substantially reduced further [15, 16]. Unfortunately, further reduction in ZDDP content below the 0.08 wt.% of phosphorus will adversely affect the tribological performance of currently used low viscosity lubricants (like GF6). Clearly, it is important to identify novel new additives capable of either replacing or at least reducing, ZDDP content in the engine oil given our increasing concern over energy consumption and undesirable climate effects.

To this end, in recent years, various nanomaterials have been explored as additives in lubricant base oil from the perspective of developing more energy-efficient lubrication to impart superior tribological performance and lower emissions than conventional additives like ZDDP [17–25]. The integration of nanomaterials into tribological systems has several benefits over their micron-sized counterparts, for example, their extremely small size and high specific surface area [26]. Nanoscale materials are believed to involve a different mechanism for friction and wear reduction compared to P-based lubricant additives. For example, metal and metal oxide nanoparticles may get physically pressed, or smeared on the rubbing surfaces, at high contact pressure to form protective surface layers or tribo-sintered films, which decrease resistance to shear stress and provides a cushion against direct asperities collision [19, 26, 27]. Hard carbon-based or ceramic particles are reported to act as mini-ball bearings at the sliding interface [28, 29]. On the other hand, soft carbon-based nanomaterials exfoliate to form a protective film upon rubbing [30–32].

Calcium carbonate nanoparticles are of our particular interest given their excellent chemical stability, frictional and wear reduction properties, and potential as a green lubricant additive in commercial oils [33–36]. Practical lubrication applications of metal oxide nanoparticles face major challenges, such as agglomeration and sedimentation in the base oil. To help overcome these effects, several studies have shown the efficacy of using surface modifications to improve the solubility of metal oxide nanoparticles in oils [18, 37–40].

In the present study, we report tribological results from $CaCO_3$ nanoparticles surface modified with two coatings, one to assist in the film formation and the other to resolve the dispersion problem achieved via a plasma-enhanced chemical vapor deposition (PECVD) technique coating process. The 1st film involves a coating that permits nanoparticles to deposit tribologically beneficial chemistries at sliding interfaces to promote the formation of the tribofilms. The second coating, involving the deposition of hydrophobic films, is employed to ensure that the nanoparticles will disperse uniformly in the oil. To this end, $CaCO_3$ nanoparticles were coated with boron-based polymer films, followed by the second film of a polymeric acrylate-based film on top of the boron-coated $CaCO_3$ nanoparticles ($CaCO_3$BM). Subsequently, the plasma functionalized calcium carbonate nanoparticles were characterized using Fourier transform infrared spectroscopy (FTIR) and X-ray absorption near-edge structure (XANES) spectroscopy.

The main objective of this study was to assess the feasibility of these plasma functionalized $CaCO_3$BM nanoparticles to help reduce the amounts of phosphorus currently employed in engine oils. Specifically, we focused on reducing the amount of P to 350 ppm, approximately half of that currently employed commercially with zinc dialkyl dithiophosphate (ZDDP) and ashless dialkyl dithiophosphate (DDP) additives. For this purpose, oil formulations were prepared with $CaCO_3$BM nanoparticles in combination with/without ZDDP and DDP, and tribological properties were assessed through high frequency reciprocating tribometer under the boundary lubrication regime. In addition to friction and wear properties, electrical contact resistance data were acquired *in-situ* during tribological tests to evaluate the dynamics of tribofilm formation at the sliding interface. Subsequently, surface characterization techniques, including atomic force microscopy (AFM) and XANES, were employed to determine the morphology and chemical make-up of the tribofilms. The results obtained provide interesting fundamental new insights into the anti-wear mechanism and nature of the tribofilm formed, along with encouraging evidence of possible reduction of phosphorus content in the oil.

2. Experimental Details

2.1 Materials

The $CaCO_3$ nanoparticles, of size 30–40 nm, were obtained from the Sky Spring Nanomaterials. For plasma functionalization of $CaCO_3$, the monomer precursors trimethyl boroxine, and glycidyl methacrylate monomers utilized were purchased from Sigma Aldrich, as analytical grade reagents, and were employed without further purification. Test lubricants were formulated using ZDDP and DDP phosphorus-based anti-wear additives in Group III mineral base oil. Group III mineral base oil (Viscosity @100ºC – 4cst) was procured from GS Caltex, while ZDDP and DDP additives were obtained from Oronite and BASF respectively. The chemical structure of all anti-wear additives used in this study is shown in Table 1.

Table 1 The coded names, structure, and chemical names of anti-wear additives

Code	Chemical name	Structure	Wt.% P
DDP	Ashless dialkyl dithiophosphate	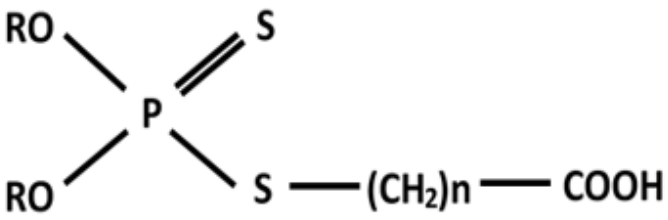	9.3
ZDDP	Zinc dialkyl dithiophosphate	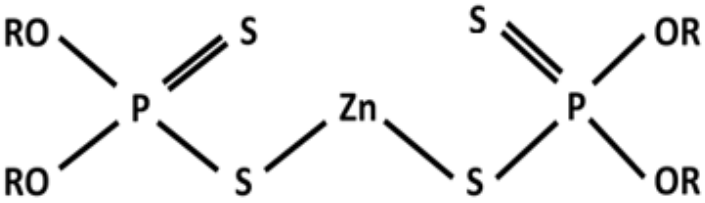	7.27
$CaCO_3$BM	Plasma functionalized $CaCO_3$ nanoparticles	 Coating from Trimethyl boroxine Coating from Glycidyl Methacrylate	N/A

2.2 Preparation of functionalized $CaCO_3$ nano-additives and test lubricants

Core-shell structure functionalized $CaCO_3$ nanoparticles were synthesized via a plasma processing technique, specifically plasma-enhanced chemical vapor deposition (PECVD). A home built 360° degree continuously rotatable plasma reactor was used in this study to ensure uniform and efficient coating of the $CaCO_3$ nanoparticles. It was observed that the continuous rotational motion of the reactor was effective in assuring dispersion of the nanoparticles in the gaseous plasma discharge, thus continuously exposing fresh $CaCO_3$ surfaces to the plasma generated reactive species. Initially, 3g of $CaCO_3$ nanoparticles were loaded inside the borosilicate glass reactor and were exposed to a plasma generated with trimethyl boroxine monomer. This deposition process was carried out using a continuous wave (CW) plasma for as initial 20 mins, followed with pulsating wave plasma (PW) generated with sequentially reducing duty cycle from 20:30 (plasma on time: plasma off times in seconds) to 20:60, for 10 minute

periods at each ratio. The technique of using both CW and PW plasma to achieve adhesive polymer film is reported in our previous work [41–43]. The monomer pressure was maintained at 120 mT and RF power was kept at 60 W throughout the process. To facilitate effective chemical characterization of plasma polymer films, Fourier transforms infrared (FTIR) analysis was carried out on trimethyl boroxine films deposited on flat substrate KBr cards and Si wafers. Additionally, to confirm the uniform deposition of plasma polymer films on nanoparticles, $CaCO_3$ nanoparticles exposed to trimethyl boroxine monomer were characterized using the X-ray absorption near edge (XANES) technique. XANES boron K-edge spectra, shown in Fig. 1(b), exhibit the presence of boron-based films on the surface of $CaCO_3$ nanoparticles. Subsequently, methacrylate-based polymer films were deposited on the top of boron-based coatings to assist the dispersion of the $CaCO_3$ nanoparticles in the base oil. For this purpose, glycidyl methacrylate monomer was used and the deposition process was carried out using 100 W, monomer pressure of 70 mT, continuous-wave plasma – 20 min, pulsating plasma with a duty cycle (20:50) – 40 min.

Table 2
Test lubricant details and additive composition

Coded name	Lubricant	Additive Composition
BO	Group III mineral base oil	No additives were added
$CaCO_3$BM	Plasma functionalized $CaCO_3$ mixed with group III mineral base oil	$CaCO_3$BM – 0.5 wt.%
ZDDP350	Zinc dialkyl dithiophosphate mixed with group III mineral base oil	ZDDP – 0.035 wt.% of P
DDP350	Ashless dialkyl dithiophosphate mixed with group III mineral oil	DDP – 0.035 wt.% of P
ZDDP350_$CaCO_3$BM	Plasma functionalized $CaCO_3$ mixed with ZDDP in group III mineral base oil	$CaCO_3$BM – 0.5 wt.% ZDDP – 0.035 wt.% of P
DDP350_$CaCO_3$BM	Plasma functionalized $CaCO_3$ mixed with DDP in group III mineral base oil	$CaCO_3$BM – 0.5 wt.% DDP – 0.035 wt.% of P
ZDDP700	Zinc dialkyl dithiophosphate mixed with group III mineral base oil to mimic commercial oils	ZDDP – 0.07 wt.% of P

Different oil formulations were prepared by mixing functionalized $CaCO_3$BM nanoparticles in mineral group III base oil to assess their anti-wear and anti-friction performance. Initially, tribological tests were conducted to determine the optimum concentration of nano-additives by using oils containing non-

functionalized $CaCO_3$ nanoparticles at different concentrations (0, 0.3, 0.5, 1 wt %), the results of which are shown as a bar graph in Fig. 1(c). Based on the friction and wear results of the concentration test, $CaCO_3$BM nanoparticles were added to the base oil at a 0.5 wt.% percolation threshold. Table 2 details the coded name and concentration of additives employed to prepare the six oil formulations.

The 0.5% P-containing additives added to the base oil represent 350 ppm of P concentration, a significant reduction compared to the 700–800 ppm of P used in conventional engine lubricants, Probe sonication for 15 min was employed to ensure homogenous mixing of $CaCO_3$BM, ZDDP, and DDP additives in the base oil. Functionalized $CaCO_3$BM nanoparticles retained dispersion in the base oil for over a month of observation time.

2.3 Tribological Tests and Worn Surface Characterization

A linear reciprocating tribometer with the cylinder-on-flat configuration at Argonne National Laboratory was employed to evaluate the tribological performance of the oil dispersed with or without functionalized $CaCO_3$ additives and base oil. Tests were performed with an AISI 52100 steel cylinder (4mm × 6mm) reciprocating or sliding against an AISI 52100 steel flat (12mm × 12mm × 4mm). The upper cylinder was a standard grade bearing steel of surface roughness ~ 15 nm (Sa) and the hardness was measured to be ~ 60 HRc. The steel flat surface was polished using 1200 grit SiC abrasive paper to reach a roughness of ~ 12 nm (Sa) and the hardness was measured to be in the range of 58–60 HRc. All contact surfaces were thoroughly cleaned with Stoddard solution, isopropanol, and acetone before the test. Tribological tests were conducted at 100 ºC temperature under a normal load of 82 N and speed of 300 rpm and 6mm stroke for a sliding duration of 60 min. These test parameters were selected to closely simulate the contact pressure and sliding speed experienced at the cylinder liner-piston ring interface in the internal combustion engine. Lubricant film thickness was calculated using the Dowson-Higginson equation [44] to ensure all tests were run under the boundary lubrication regime. Three replicates were run for each lubricant. After completion of the tests, both cylinder and flat samples were cleaned using heptane to remove oil residue and were preserved for tribofilm characterization in additive-free poly-alpha olefin oil. The coefficient of friction data was measured in-situ during tribological tests using DasyLab software. The non-contact 3D optical profilometer and optical microscope were used to measure the wear volume of cylinder test samples.

Worn surfaces generated on the steel flat samples were subjected to extensive surface characterizations. The morphology and topography of interfacial tribofilms formed by additives were elucidated through analysis of worn surfaces generated on flat test specimens using atomic force microscopy (AFM). The high-resolution imaging capability of AFM allows us to acquire the 3D morphology of tribofilms at nanometer-scale resolution. AFM was used in the contact mode to obtain 3D scanning probe microscopic images of the rubbed surfaces detailing wear characteristics and mechanism in play at the tribological contact.

X-ray absorption near edge spectroscopic (XANES) was employed to determine the chemical make-up and properties of the tribofilms. XANES characterization was carried out at the Canadian Light Source

synchrotron facility. For XANES analysis, flat steel samples were cleaned thoroughly using isopropyl alcohol and then loaded inside the vacuum chamber. Each sample was scanned at two different spots (left edge, or right edge, and center area of the wear scar) to ensure consistency in the results. The phosphorus L-edge and boron K-edge data were collected at a variable line spacing plane grating monochromator (VLS-PGM), operating at the energy range from 5.5 eV to 250 eV, with a photon resolution of more than 10000 E/ΔE. The phosphorus, calcium, and sulfur K-edge data were acquired at a soft X-ray micro characterization beamline (SXRMB), which provides an energy range from 1.7 keV to 10 keV and a photon resolution of more than 3.3 x 10 − 4 InSb (111). The zinc L-edge, iron L-edge, and oxygen K-edge spectra were acquired at a spherical grating monochromator (SGM) beam station operating at the energy range of 250–2000 eV and a photon resolution of more than 5000 E/ΔE. Spectra at both VLS-PGM and SGM beam stations were collected using 100 µm × 100 µm beam spot size, while the large spot size of 1 mm × 2 mm was used at the SXRMB beam station. Both high energy K-edge and low energy L-edge spectra were acquired in the total electron yield (TEY) and fluorescence yield (FY), two different detection modes. TEY mode provides chemical information of the surface layers/ near-surface region whereas the FY mode detects information from the bulk of the sample. For example, the sampling depth of P L-edge TEY mode is only ~ 5 nm, while in P L-edge FY mode ~ 60 nm of the bulk of the sample is probed.

3. Results And Discussion

3.1 Coefficient of Friction and Wear Volume

The coefficient of friction (COF) data recorded *in-situ* during the tribological test is plotted in Fig. 2 as the function of test time for all formulations. The average coefficient of friction of three repeat runs is also provided in Fig. 3. Error bars in Fig. 3 represents the standard deviation between the average COF of three repeat runs. Variance in the friction profile helps to indicate the presence or removal of smooth surface providing low shear strength at tribological contacts. The friction profile of the sample (A) BO exhibits unstable and high values of COF throughout the completion of tests. On the other hand, the friction response of sample (B) $CaCO_3$BM is relatively stable. For the first 25 min of sliding, rapid increase and drop in COF values are observed, but as the test continues COF value drops and becomes stable. Surprisingly, the ZDDP sample exhibits the most dramatic friction response, wherein for the initial 15 min some variance and high COF are observed, but after that COF values drop and increase and for the last 25 min becomes stable. Interestingly, sample (E) with the combination of ZDDP and $CaCO_3$BM exhibits lower COF values than the sample (C) with only ZDDP. Sample (F) with the mixture of ZDDP and $CaCO_3$BM nanoparticles exhibits the steadiest friction response of all, however, COF values near the end of the test are slightly higher than the COF values for sample (B) with only $CaCO_3$BM and sample (D) with only DDP. It is important to note that after 40 min of the test, the friction profile for samples (B), (D), (E), and (F) appears to be stable and similar with low COF values. The stability in the friction profile indicates that the boundary tribofilms formed by these additives are very robust under applied normal load

and high contact pressure. As shown in Fig. 3, oil formulations containing only $CaCO_3$BM, only ZDDP, and only DDP exhibits the highest average COF value, while binary additive formulations containing $CaCO_3$BM with ZDDP and DDP display the lowest average COF values. Notably, DDP_$CaCO_3$BM exhibits lower COF than ZDDP_$CaCO_3$BM. Overall, these data indicate that the addition of $CaCO_3$BM to ZDDP and DDP results in an improvement of friction response, even slightly better than the sample with 700 ppm P.

The wear performance of $CaCO_3$BM nano-additives and binary additive mixtures of $CaCO_3$BM with ZDDP and DDP was benchmarked against the oil containing only ZDDP and only DDP additives. To assess wear appearance and surface deformation on worn surfaces, 3D surface profilometry images of the area of contact of cylinder sample were procured through profilometer, which is added in the Supporting Information section for reference. Wear volume results of cylinder test specimens, measured using an optical profilometer, are displayed in Fig. 4. The black color error bar on the bar chart represents the standard deviation of wear volume results of three repeat tests for each formulation. BO test oil exhibits the highest volume loss on the cylinder whereas the addition of both nano-additives and P-containing additives to the base oil led to a significant reduction in wear. Notably, the addition of plasma functionalized $CaCO_3$BM resulted in an 89.37% improvement in the wear performance of base oil. Interestingly, sample (C) with ZDDP at 350 ppm exhibited increased wear as compared to sample (D) with DDP at 350 ppm of P level.

The mixture of $CaCO_3$BM with ZDDP and DDP (i.e. sample (E) and (F)) resulted in significant improvement in wear performance indicating synergistic interaction of developed $CaCO_3$BM nanoparticles with ZDDP and DDP. It is important to note that formulation (F) of $CaCO_3$BM and DDP resulted in the lowest wear volume compared to all other formulations, even slightly better than the ZDDP sample with 700 ppm P. Additionally, wear performance was assessed by mathematically calculating volume loss of cylindrical test specimens using optical microscopy. These results are similar to wear inferences derived from the profilometry results and are therefore not included here. Optical microscopic images of wear scar generated on the cylinder and flat test specimen are provided in the supporting information section. Wear surfaces on both cylinder and flat as shown in figure S2 and S3 have visually distinguishable features that reveal the formulation with an additive mixture of $CaCO_3$BM and DDP offered excellent wear protection compared to other lubricants. Clearly, the overall friction and wear results highlight the advantage of extra chemistries deposited by $CaCO_3$BM in enhancing tribological properties without relying on reduced phosphorus concentration.

3.2 Tribofilm formation using electrical contact resistance

The high-frequency reciprocating rig tribometer used in this study was equipped with an electric setup design to record electrical contact resistance (ECR) across the counter bodies. Many researchers have shown that a highly resistive film is formed by P-based additives during the rubbing process and have successfully used the ECR technique to detect the presence, or absence, of lubricating films at tribo-contacts [45, 46]. In the present study, 1 mA direct current was applied between countersurfaces of a steel cylinder (positive) and steel flat (negative) to record ECR measurements.

At the beginning of the test, when the steel cylinder slides against flat and no tribofilms has formed, the resistance of the circuit is low, and the voltage drop value is close to 0 mV. As the rubbing continues, insulating tribofilms are formed which causes an increase in resistance of the circuit and the voltage drop value shoots up close to 100 mV. In this way, measurement of ECR *in-situ* during tribological tests allows to effectively analyze overall dynamics of tribofilm formation. Importantly it helps to determine the incubation time required for anti-wear additives to form tribofilms at the interface.

Figure 5 shows ECR voltage drop signals plotted as the function of test time. Data points near 0 mV correspond to no tribofilm and near 100 mV to the presence of effective tribofilm. Sample (a) with functionalized $CaCO_3$BM nanoparticles exhibits the majority of data points in the upper half of the plot, apparently suggesting the formation of a thin protective film by nanoparticles at the interface after 15 min of sliding. In the case of ZDDP sample (b), data points appear to be dispersed for the first 15 min and after that are segregated near 100 mV. This indicates that tribofilms were forming and gradually breaking down during initial rubbing while later stability was achieved and maintained throughout the test. For sample (c) with DDP, tribofilm formation begins after 5 min of rubbing as opposed to 15 min sample (b) ZDDP. Additionally, tribofilms formed by DDP appears to be stable for the majority of test time with some minor breakdowns. Surprisingly, the voltage data points for the sample with a mixture of $CaCO_3$BM and ZDDP appear to be dispersed initially but after ~ 5 min numerous data points are close to 100 mV compared to sample (b) with only ZDDP, thus indicating that boron coated $CaCO_3$ nanoparticles available at the interface promote highly stable tribofilms of ZDDP even at a lower concentration of 350 ppm of P. Thus, ECR data for samples with an additive mixture of $CaCO_3$BM and ZDDP compliments wear volume results discussed in Sect. 3.1. Additionally, the ECR plot of sample (e) is drastically different from the ECR plot of sample (c). Data points for sample DDP_$CaCO_3$BM reaches a maximum value in a slightly early stage and remains relatively more stable than the sample with only DDP. These differences in incubation time and stability further supports that developed $CaCO_3$BM nano-additives interact synergistically with ZDDP and DDP additives and form robust tribofilms leading to enhanced anti-wear protection of boundary lubricated contacts.

3.3 Morphology and Topography of Tribofilms

AFM was used to observe and compare general topographical and morphological features of tribofilms formed due to the interaction of $CaCO_3$ nano-additives with ZDDP and DDP. Figure 6 shows AFM images of the 45 μm × 45 μm area probed around the wear scar along with the scale bar. Each sample was scanned at four spots close to the center region, while only one representative scan is shown in Fig. 6. It is apparent from all AFM images that, in both nano-additives and P-containing additives, a tribofilm is formed obscuring visibility of the ground steel surface. Looking first at the $CaCO_3$BM, AFM image reveals several discrete small tribofilms or pad-like features, along with evidence of directionality. It appears that pads are elongated in the direction of sliding. This nanoparticle reinforced tribofilm exhibits thinner and slightly rougher surface characteristics than ZDDP and DDP tribofilms. 3D topographical image of the ZDDP sample exhibits the presence of relatively homogenous tribofilms with thin and elongated pads oriented in the sliding direction. These films have uniformly elevated features and appear to be smoother

than $CaCO_3$BM. The observed morphology of ZDDP tribofilms resembles ZDDP films reported in the literature by various authors [47–51]. AFM image of the DDP sample as shown in Fig. 6(c) reveal that the surfaces of these tribofilms are quite heterogeneous, with the combination of large and small size pads. However, it should be noted that the pads formed by DDP have a higher thickness and are covering a larger area than the pads formed by ZDDP. Najman et al. studied tribological properties

of extreme pressure organo-sulfur additives and correlated poor anti-wear performance of additives to the formation of tribofilms containing smaller pads [52]. Similarly, here the better wear volume results of DDP than ZDDP can be associated with the formation of wider and thicker pads. Interestingly, surface characteristics of tribofilms formed due to interaction of $CaCO_3$BM and ZDDP exhibit better coverage of tribofilms with pad size larger than what is seen in the case of only ZDDP lubricated sample. Also, pads are continuous and elongated in the direction of sliding. Some areas of this sample appear to have deeper scratches in the sliding direction. On the contrary, surface lubricated with $CaCO_3$BM and DDP combined additive mixture reveal the best coverage of patchy tribofilms covering rough surface asperities. Although the pad appears to be smaller in diameter, the height (/thickness) of the pads are like that of the ZDDP_$CaCO_3$BM tribofilm sample. These topographical differences indicate the benefit of synergistic interaction of functionalized $CaCO_3$BM and DDP and/ ZDDP in strengthening properties of tribofilms and enhancing wear protection at the tribological interface.

3.4 Tribochemical analysis using XANES

3.4.1 XANES K-edge characterization

Calcium K-edge

To interpret the role of $CaCO_3$BM nanoparticles in promoting tribofilm formation and confirm interaction with P-based additives, calcium K-edge FY absorption spectra for all samples were recorded and compared with model compounds $Ca_2P_2O_7$, CaO, $CaCO_3$, $CaHPO_4$, $Ca_3(PO_4)_2$ as shown in Fig. 7(a). Ca K-edge FY has three characteristic discernable peaks labeled as **a**, **b**, and **c**. Details on peak position and electronic transitions can be found elsewhere [53, 54].

The Ca K-edge spectra of $CaCO_3$BM nanoparticles-based lubrications reveal the presence of calcium chemistry on the tribo-surface. It is evident from these plots, that the sample with only

Fig. 7 XANES K-edge characterization of tribofilms formed by all prepared oil formulations detailing information on (A) Calcium K-edge TEY; (b) Boron K-edge FY; (c) Phosphorus K-edge TEY; (d) Sulfur K-edge FY

$CaCO_3$BM has its pre-edge peak **a** aligned exactly with the $CaCO_3$ model compound, whereas its main peak position is between the white line of $CaCO_3$ and CaO, which indicates a small contribution from CaO to the chemical makeup of tribofilms while the majority of calcium is associated with $CaCO_3$ in these tribofilms. The peak positions and intensities in FY spectra of ZDDP_$CaCO_3$BM and DDP_$CaCO_3$BM

reveal the presence of calcium phosphates in the tribofilms. It is difficult to distinguish among the calcium phosphate compounds, however, careful observation of peak **b** hints at the presence of $CaHPO_4$ in both tribofilms.

Boron K-edge

Boron K-edge was acquired for all formulations to confirm the capability of plasma functionalized $CaCO_3$BM nanoparticles to deliver coated boron chemistries at the tribological interface. Boron K-edge FY spectra of tribofilm samples compared with model compounds in Fig. 7(b) reveal important information on the co-ordination and intermediate-range structure of B in the tribofilms. Boron K-edge FY spectra exhibit characteristic three peaks **a**, **b**, and **c**. Peak **a** at 194.0 eV and **c** at 203 eV are attributed to boron in trigonal co-ordination, while peak **b** at 198.4 eV corresponds to boron in tetrahedral co-ordination [55, 56]. Spectra of B_2O_3 and H_3BO_3 are signatures of boron in trigonal co-ordination. On the other hand, the spectrum of BPO_4 represents boron in the tetrahedral form wherein small intensity peaks **a** and **c** possibly originates from surface modification. From Fig. 7(b) it is evident that, in the absence of ZDDP and DDP additives, $CaCO_3$BM forms tribofilms mainly composed of trigonal boron species. FY spectrum of sample $CaCO_3$BM exhibits a strong intensity peak **a** indicating that boron is present in the form of H_3BO_3/B_2O_3 in the tribofilm. Additionally, there is a low-intensity noisy peak **b** possibly suggesting that partial transformation might have occurred to produce tetrahedral boron species. Zhang et al. also reported that in tribofilms formed by borated additives, boron species transformed from trigonal co-ordination to tetrahedral co-ordination on rubbing [57]. The spectrum of the sample with $CaCO_3$BM and ZDDP appears to be quite different than the spectra of model compounds. This spectrum exhibits a strong intensity peak at 196.7 eV and a shoulder on the lower energy side at 194.6 eV which corresponds to trigonal boron in H_3BO_3 and B_2O_3. Here, the 196.7 eV peak is in between peak **a** and peak **b**. This unique peak position indicates the presence of a complex metal borate calcium, zinc, and iron species, also present in this tribofilm [58, 59]. Interestingly, the blending of $CaCO_3$BM and DDP additives has resulted in different boron chemistries and distinct boron K-edge spectrum. The strong intensity peak at 193.3 eV matches with iron borates ($Fe_2Fe^{3+}BO_5$) in the literature [60] whereas the low-intensity shoulder around 195.5 eV corresponds to P 2s from the phosphate structure [61]. As the cross-section of B 1s is much larger than that of P 2s, B K-edge XANES peaks are at a higher intensity (i.e. peak at 193.3 eV) than the P 2s peak [61]. The P L-edge FY results (discussed later) suggests that these tribofilms contain $FePO_4$ and therefore, the shoulder around 195.5 eV seen in Fig. 7(b) can be assigned to $FePO_4$ present in the bulk of tribofilms.

Phosphorus K-edge

XANES phosphorus K-edge TEY spectra of tribofilm samples and model compounds, BPO_4, $Ca_3(PO_4)_2$, $FePO_4$, and $Zn_3(PO_4)_2$ are displayed in Fig. 7(c). The main absorption peak in the P K-edge spectra arises due to the transition of an electron from phosphorus 1s orbital to unoccupied 2p orbital. The main absorption peak **b** of $FePO_4$ is at slightly higher energy than peak **a** of $Zn_3(PO_4)_2$ and $Ca_3(PO_4)_2$ model compounds. Additionally, $FePO_4$ has distinctive pre-edge peak **a'** which is absent in $Zn_3(PO_4)_2$ and

$Ca_3(PO_4)_2$. $Ca_3(PO_4)_2$ has a unique shoulder after the main absorption peak and BPO_4 has the main absorption edge at a higher energy level than $FePO_4$. Tribofilm samples from ZDDP and DDP contain iron phosphates as the main absorption peak which exactly matches with peak **b** of $FePO_4$. The tribofilms formed due to the interaction of $CaCO_3$BM and ZDDP do not contain iron phosphates as the pre-edge peak **a'** is missing and the peak **b** of FePO4 does not match that of the tribofilm. The high-intensity peak aligns with peak **a** and thus, indicates the dominance of $Zn_3(PO_4)_2$ in the chemical make up of these surface films. Phosphorus K-edge TEY spectra of DDP_$CaCO_3$BM sample exhibits peak position and features similar to TEY spectrum of $FePO_4$ model compounds and thus, indicates that these tribofilms are mainly comprised of iron phosphates in the bulk. Both ZDDP and DDP, when mixed with CaCO3BM nano-additives, give rise to zinc phosphate and iron phosphate-based tribofilms respectively and there is no formation of boron phosphate. Thus, the P K-edge results indicate that the boron chemistry from the shell of $CaCO_3$BM nanoparticles has no influence on the chemical environment of phosphorus in the tribofilms. However, Ca K-edge FY spectra for ZDDP_$CaCO_3$BM and DDP_$CaCO_3$BM do reveal the presence of calcium phosphate in the bulk of the tribofilms, suggesting that the core of $CaCO_3$BM nanoparticles does react with decomposition products of ZDDP and DDP. P K-edge FY spectra acquired for all samples were very similar to spectra obtained in TEY mode and hence, are not discussed here.

Sulfur K-edge

Sulfur K-edge is sensitive to oxidation states of sulfur and is useful in determining sulfur species in samples containing complex compositions. Sulfur K-edge FY spectra for model compounds, shown in Fig. 7(d) have characteristic peaks **a**, **b**, and **c**. The main absorption peak of sulfides is at lower photon energy i.e. FeS_2 (peak **a**) is at 2471.5 eV, and ZnS (peak **b**) is at 2473 eV. The peak positions for sulfate compounds $ZnSO_4$, $FeSO_4$, and $Fe_2(SO_4)_3$ are at higher energy, around 2482 eV. Tribofilms formed by all oil formulations has sulfur in several oxidation states, as evident from peaks **a**, **b**, and **c**. The spectrum for the ZDDP sample has features similar to the ZnS model compound with the presence of additional peak **c** corresponding to the $ZnSO_4$ compound. This suggests zinc sulfide is the main chemical state of sulfur with a minimum concentration of zinc sulfates in these tribofilms. Likewise, the sulfur K-edge plot for ZDDP_$CaCO_3$BM has its main feature aligned with ZnS. Looking at the XANES spectrum of DDP, we can see that peak **a** and **c** aligns perfectly with FeS_2, whereas the FY spectrum of DDP_$CaCO_3$BM has a high-intensity peak and mid-intensity peak (marked by dotted lines) at 2477.7 eV, which matches with a characteristic peak position of FeS in the literature [62]. Also, there is a low-intensity shoulder on the higher energy side of peak c' which can probably be attributed to a minor concentration of iron sulfates. These observations indicate that sulfur from the decomposing DDP additive reacts with iron or surface oxide to produce iron sulfide. This iron sulfide can then react partially with oxygen or iron oxide to form some sulfate (and sulfite) as in the case of DDP_$CaCO_3$BM.

3.4.2 XANES L-edge characterization

Phosphorus L-edge

The phosphorus L-edge TEY and FY spectra of tribofilms are plotted along with model compounds FePO4, $Zn_3(PO_4)_2$, $Ca_3(PO_4)_2$, and BPO_4 and are shown in Fig. 8(a) and 8(b), respectively. Compared to phosphorus K-edge, phosphorus L-edge provides detailed chemical information of near-surface region ~ 5 nm and of bulk ~ 60 nm depth of tribofilm. Additionally, phosphorus L-edge spectra help to determine the chain length of polyphosphate glasses present on the sample surface. The L-edge spectra are characterized by peaks **a**, **a′**, **b**, **c**, and **c′**. Details on these peak positions and electronic transitions can be found elsewhere [63, 64].

The TEY spectrum of ZDDP exhibits the strong presence of zinc phosphates at the near-surface region while, interestingly, the FY spectrum of this sample shows a very strong intensity

Fig. 8 XANES L-edge characterization of tribofilms formed by all prepared oil formulations detailing information on (a) Phosphorus L-edge TEY; (b) Phosphorus L-edge FY; (c) Iron L-edge TEY

peak at **c′** thus revealing the presence of iron phosphates in the bulk of these tribofilms. In contrast, the phosphorus L-edge TEY and FY spectra of DDP reveal a strong presence of iron phosphates throughout the surface and to the bulk of the tribofilms. TEY spectra for tribofilms generated with ZDDP_$CaCO_3$BM based lubrication exhibit a strong main absorption peak, aligned to that of the $Zn_3(PO_4)_2$ model compound. However, its corresponding FY spectra display a high-intensity characteristic peak in between **c** and **c′** peaks, thus indicating that the mixture of zinc phosphates and iron phosphates are present in the bulk of these tribofilms.

The chain length of detected zinc and iron phosphate glass can be determined from phosphorus L-edge spectra by calculating the ratio of intensity of **a**/**a′** peak to peak **c**/**c′** [65, 66]. The chain lengths are mentioned next to the respective spectrum in Fig. 8(a). An a/c ratio of less than 0.40 represents the presence of short-chain length polyphosphate glasses, while a chain length greater than 0.70 suggests long-chain polyphosphate glass [67]. A film with an a/c ratio between 0.40 and 0.60 is termed a medium-chain polyphosphate [68]. From a/c values in Fig. 8(a), it is evident that the interaction of $CaCO_3$BM nano-additives with ZDDP and DDP is resulting in the formation of tribofilms with increased chain length than the oils containing only ZDDP and DDP.

Iron L-edge

The Fe L-edge TEY spectra provide some vital information regarding the iron atoms present in the tribofilms for different test samples. From Fig. 8(c), we see that the L-edge spectra of model compounds display two main peaks at 707.1 eV and 708.5 eV, irrespective of the oxidation state of Fe. The splitting and intensity ratios between the two main peaks are attributed to the interplay of crystal-field, spin-orbit, and electronic interactions (Coulomb and exchange) [69]. The most intense peak is used for fingerprint analysis i.e. to detect Fe^{2+} or Fe^{3+} compounds in the tribofilm sample. It is important to note that the intensity of the second peak increases noticeably when the oxidation states of iron are increased from Fe^{2+} to Fe^{3+}. The spectrum of the $CaCO_3$BM sample exhibits main absorption peaks in alignment with the

Fe_2O_3 model compound. The characteristic splitting, as seen in the spectrum of both ZDDP and ZDDP_$CaCO_3$BM samples, is almost the same, showing a slightly higher intensity of Fe^{2+} peak. This indicates that these tribofilms are comprised of a mixture of different iron phosphates with a slightly major concentration of $Fe_3(PO_4)_2$. Fe L-edge spectra of the DDP sample show the main intensity peak at 708.5 eV highlighting the strong presence of $FePO_4$ phosphates in the tribofilm. Interestingly, the interaction of DDP and $CaCO_3$BM has resulted in the formation of tribofilms containing $Fe_3(PO_4)_2$, as the main absorption peak and overall features of the samples Fe L-edge spectrum matches with the $Fe_3(PO_4)_2$ compound. It is important to note that there might be a minor concentration of Fe_2O_3 present in the tribofilms formed with lubricants containing ZDDP and DDP additives, as the characteristic peak of Fe_2O_3 overlaps with the main absorption peak of these tribofilm samples. From the analysis of Fe L-edge spectra of all tribofilm samples, it can be concluded that iron is majorly associated with phosphorus and not with the sulfur at ~ 50 nm beneath the top surface.

3.5 Discussion on Tribofilm formation and Wear Reduction Mechanism

This study has confirmed the ability of boron coated $CaCO_3$BM nanoparticles to interact synergistically with P-based additives to form thick tribofilms and improve anti-wear performance under comparable boundary lubrication conditions. Our aim was not just to attempt to reduce the phosphorus oil additives but also to further understand the tribofilm formation and anti-wear mechanism of the developed binary additive system of $CaCO_3$BM and P-based anti-wear additives. The XANES and microscopic data obtained are utilized in our attempt to pictorially illustrate the

various tribofilms formed during this work, as shown in Fig. 9. In general, there are four feasible lubricating mechanisms for metal nano-additives: a) Ball bearing effect- where spherical nanoparticles act like tiny ball bearings at the contact zone and change sliding motion to roll, thereby reducing the effective COF; (b) polishing effect- Hard nanoparticles smoothen off the surface asperities to reduce the roughness of the lubricating surface and improve tribological characteristics; (c) mending effect- nanoparticles deposit or fill the grooves and scars on the tribo-surface and compensate for the material loss; (d) Tribofilm formation- nanoparticles under high temperature and pressure get smeared or compacted to form adsorbed or tribo-sintered films or nanoparticles which allows decrease resistance to shear for lower friction and prevent direct metal-metal contact to reduce wear. In this study, a functionalized $CaCO_3$BM nanoparticles bearing effect was not observed since the worn surfaces produced with $CaCO_3$BM nanoparticles were slightly rougher. XANES analysis and comparison in Figs. 7 and 8 reveal that $CaCO_3$BM nanoparticles form tribofilms containing iron borates, B_2O_3, H_3BO_3, CaO, $CaCO_3$, and iron oxides. Zhang et al reported the tribological behavior of the $CaCO_3$ nanoparticles in PAO base oil and using XPS revealed the deposition of similar tribofilms enriched with $CaCO_3$ on contact surfaces leading to friction and wear reductions [34]. The phenomenological model of tribofilms formed with $CaCO_3$BM as shown in Fig. 9(a) exhibits boron-based compounds near the sliding surface while the top surface of tribofilm patches is dominated by Ca-based compounds. This indicates that the boron

chemistry was provided at the tribological surface through the removal of the outer polymer shell of $CaCO_3$BM nanoparticles under high tribo-stresses. Additionally, the presence of calcium oxide and iron borates in the tribofilms indicates that nanoparticles contributed to tribofilm formation through a chemical reaction and not simply by mechanical mixing.

Tribo-chemistry plays a vital role in determining mechanisms of action of anti-wear additives. Here, Fig. 9(b) exhibits the chemical makeup of tribofilms formed due to the interaction of $CaCO_3$BM and ZDDP, wherein the bottom layer close to steel substrate is comprised of iron oxides and iron and/ zinc sulfides/sulfates. The topmost region is dominated by medium-chain zinc phosphates with the presence of iron phosphates, calcium phosphates, and metal borates near the bulk region of the film. In contrast, the tribofilm model formed due to the interaction of $CaCO_3$BM with DDP, as shown in Fig. 9(c), is slightly different. These tribofilms are comprised of medium and short-chain length iron phosphates both in the near-surface and bulk of tribofilms, along with the iron borates. These differences in the tribo-chemistry support the previous tribofilm forming mechanism, proposed for both ZDDP and DDP [11, 15, 68, 70–73]. ZDDP is well-known to decompose and then self-react to deposit a tribofilm primarily composed of zinc and iron phosphates and oxides [9, 48, 74]. Such a mechanism does not apply to ashless DDP additive because they do not self-supply metal cations [68]. The two apparent sources of Fe cation supply for DDP are the contact surface and wear debris and therefore, the tribofilms formed due to ashless DDP in Fig. 8(c) majorly contain iron-based compounds. It is important to note that, in both cases, calcium phosphates are present deeper in the tribofilm which strongly indicates that the $CaCO_3$BM nanoparticles are participating in tribofilm formation by providing stabilizing Ca cations to assist Zn or Fe in forming phosphates in the tribofilm.

ECR results exhibited that the DDP by itself forms tribofilms at a slower rate than ZDDP, however, the addition of $CaCO_3$BM nanoparticles to DDP accelerated the formation of their tribofilms. It has been reported that ashless additives forms tribofilms much slower than ZDDP because they need Fe cations by initial wear or rubbing to develop a phosphate film [73]. However, here it can be proposed that the metal cation supply through $CaCO_3$BM nanoparticles promoted the stable formation of DDP tribofilms at a faster rate. Furthermore, additional Ca and B chemistries provided by $CaCO_3$BM nanoparticles boost the thickness of ZDDP and DDP tribofilms as illustrated in AFM Fig. 6.

To evaluate the durability of nanoparticle assisted tribofilms, tribological tests were carried out with ZDDP350 and ZDDP350_$CaCO_3$BM lubricants over 2 and 4 hours of extended sliding duration. The results of these tests (summarized in Fig. 10) indicate that the tribofilms formed through the interaction of $CaCO_3$BM and ZDDP are durable and effectively protect interacting surfaces over prolonged rubbing. XANES results exhibit that after extended rubbing the outermost longer-chain polyphosphates changes to shorter chain length phosphates i.e., orthophosphates. This depolymerization of both ZDDP350 and ZDDP350_$CaCO_3$BM tribofilms is attributed to the high tribo-stresses and temperature at the tribological contacts during extended rubbing. Many studies have proposed that the chain length of zinc polyphosphates decreases with the increase in rubbing time [75]. Here, the strength/durability of the

tribofilms can be attributed to their phosphate chain length and thus change with rubbing time. Overall, it is evident from this study that the tribo-chemical reaction of $CaCO_3$BM nanoparticles with ZDDP and DDP promoted the formation of stable phosphate-rich tribofilms that lead to a corresponding improvement in tribological properties, especially wear.

4. Conclusion

In this study, surface-modified $CaCO_3$ nano-additives were synthesized using plasma polymerizations to help lower, or perhaps even eliminate, phosphorus content currently used in engine oils. The addition of functionalized $CaCO_3$BM nanoparticles in the base oil reduced friction by up to 25% and wear by up to 89% in boundary lubrication. However, when used with lower amounts of P-based additives than currently employed (i.e. 350 ppm compared to currently employed 700ppm), the $CaCO_3$BM nano-additives displayed significantly lower friction and wear values. For example, the additive mixtures of $CaCO_3$BM nano-additives with ZDDP and DDP at 350 ppm of P displayed superior tribological performance than the lubricant containing industrially used ZDDP amounts of 700 ppm of P. This significant improvement in tribological performance was attributed to the synergistic interaction of functionalized $CaCO_3$ nano-additives with ZDDP and DDP. ECR test results revealed that the interaction of $CaCO_3$BM nanoparticles with ZDDP and DDP promoted the stable formation of poly-phosphate based glassy tribofilms. Additionally, through AFM surface characterization, it was found out that for both ZDDP and DDP, the addition of $CaCO_3$BM nano-additives leads to the formation of thick patches of tribofilms, comparable to those formed by lubricants containing only ZDDP or DDP. Further, tribo-surface chemical analysis by XANES indicated that the $CaCO_3$BM nanoparticles, under high temperature and pressure conditions, formed calcium oxide and iron borate enriched tribofilms on the sliding interface. Interestingly, in the presence of ZDDP and DDP, $CaCO_3$BM nano-additives participated in the tribofilm formation by tribo-chemical reactions and Ca metal cation supply. In conclusion, the additional Ca and B chemistries provided by plasma functionalized $CaCO_3$BM nanoparticles at the tribological interface compensated for reduced phosphorus concentration in the lubricants, without adversely affecting the tribological performance.

Declarations

Acknowledgments

Tribological tests were conducted at Argonne National Laboratory. XANES experiments were conducted at the Canadian Light Source, Saskatoon, Saskatchewan, Canada that is supported by NSERC, NRC, CIHR, and the University of Saskatchewan. Support provided by the Center of Chemicals, Materials, and Biology (CCMB) at the University of Texas at Arlington is gratefully acknowledged.

References

1. Boyde, S.: Green lubricants. Environmental benefits and impacts of lubrication. Green Chem. 4, 293–307 (2002). doi:10.1039/B202272A
2. Holmberg, K., Erdemir, A.: Influence of tribology on global energy consumption, costs and emissions. Friction. 5, 263–284 (2017). doi:10.1007/s40544-017-0183-5
3. Holmberg, K., Erdemir, A.: Global impact of friction on energy consumption, economy and environment. FME Trans. 43, 181–185 (2015). doi:10.5937/fmet1503181H
4. Hsu, S.M., Zhang, J., Yin, Z.: The Nature and Origin of Tribochemistry. Tribol. Lett. 13, 131–139 (2002). doi:10.1023/A:1020112901674
5. Jaiswal, V., Kalyani, Umrao, S., Rastogi, R.B., Kumar, R., Srivastava, A.: Synthesis, Characterization, and Tribological Evaluation of TiO_2-Reinforced Boron and Nitrogen co-Doped Reduced Graphene Oxide Based Hybrid Nanomaterials as Efficient Antiwear Lubricant Additives. ACS Appl. Mater. Interfaces. 8, 11698–11710 (2016). doi:10.1021/acsami.6b01876
6. Gusain, R., Khatri, O.P.: Ultrasound assisted shape regulation of CuO nanorods in ionic liquids and their use as energy efficient lubricant additives. J. Mater. Chem. A. 1, 5612–5619 (2013). doi:10.1039/C3TA10248C
7. Bovington, C., Anghel, V., Spikes, H.A.: Predicting Sequence VI and VIA Fuel Economy from Laboratory Bench Tests. In: SAE Technical Paper. SAE International (1996)
8. Spikes, H.: The History and Mechanisms of ZDDP. Tribol. Lett. 17, 469–489 (2004). doi:10.1023/B:TRIL.0000044495.26882.b5
9. Gosvami, N.N., Bares, J.A., Mangolini, F., Konicek, A.R., Yablon, D.G., Carpick, R.W.: Mechanisms of antiwear tribofilm growth revealed in situ by single-asperity sliding contacts. Science (80-.). 348, 102–106 (2015). doi:10.1126/science.1258788
10. Mosey, N.J., Woo, T.K., Kasrai, M., Norton, P.R., Bancroft, G.M., Müser, M.H.: Interpretation of experiments on ZDDP anti-wear films through pressure-induced cross-linking. Tribol. Lett. 24, 105–114 (2006). doi:10.1007/s11249-006-9040-9
11. Zhang, J., Spikes, H.: On the Mechanism of ZDDP Antiwear Film Formation. Tribol. Lett. 63, 24 (2016). doi:10.1007/s11249-016-0706-7
12. Tse, J.S., Song, Y., Liu, Z.: Effects of Temperature and Pressure on ZDDP. Tribol. Lett. 28, 45–49 (2007). doi:10.1007/s11249-007-9246-5
13. Fujita, H., Spikes, H.A.: The formation of zinc dithiophosphate antiwear films. Proc. Inst. Mech. Eng. Part J J. Eng. Tribol. 218, 265–278 (2004). doi:10.1243/1350650041762677
14. Erdemir, A.: Review of engineered tribological interfaces for improved boundary lubrication. Tribol. Int. 38, 249–256 (2005). doi:https://doi.org/10.1016/j.triboint.2004.08.008
15. Luiz, J.F., Spikes, H.: Tribofilm Formation, Friction and Wear-Reducing Properties of Some Phosphorus-Containing Antiwear Additives. Tribol. Lett. 68, 75 (2020). doi:10.1007/s11249-020-01315-8
16. ILSAC GF-5 Standard for Passenger Car Engine Oil. (2009).

17. Uflyand, I.E., Zhinzhilo, V.A., Burlakova, V.E.: Metal-containing nanomaterials as lubricant additives: State-of-the-art and future development. Friction. 7, 93–116 (2019). doi:10.1007/s40544-019-0261-y
18. Wu, L., Zhang, Y., Yang, G., Zhang, S., Yu, L., Zhang, P.: Tribological properties of oleic acid-modified zinc oxide nanoparticles as the lubricant additive in poly-alpha olefin and diisooctyl sebacate base oils. RSC Adv. 6, 69836–69844 (2016). doi:10.1039/C6RA10042B
19. Battez, A. [Hernández, González, R., Viesca, J.L., Fernández, J.E., Fernández, J.M. Díaz, Machado, A., Chou, R., Riba, J.: CuO, ZrO2 and ZnO nanoparticles as antiwear additive in oil lubricants. Wear. 265, 422–428 (2008). doi:https://doi.org/10.1016/j.wear.2007.11.013
20. Xue, Q., Liu, W., Zhang, Z.: Friction and wear properties of a surface-modified TiO2 nanoparticle as an additive in liquid paraffin. Wear. 213, 29–32 (1997). doi:https://doi.org/10.1016/S0043-1648(97)00200-7
21. Zhou, J., Wu, Z., Zhang, Z., Liu, W., Xue, Q.: Tribological behavior and lubricating mechanism of Cu nanoparticles in oil. Tribol. Lett. 8, 213–218 (2000). doi:10.1023/A:1019151721801
22. Seymour, B.T., Wright, R.A.E., Parrott, A.C., Gao, H., Martini, A., Qu, J., Dai, S., Zhao, B.: Poly(alkyl methacrylate) Brush-Grafted Silica Nanoparticles as Oil Lubricant Additives: Effects of Alkyl Pendant Groups on Oil Dispersibility, Stability, and Lubrication Property. ACS Appl. Mater. Interfaces. 9, 25038–25048 (2017). doi:10.1021/acsami.7b06714
23. Tunckol, M., Durand, J., Serp, P.: Carbon nanomaterial-ionic liquid hybrids. Carbon N. Y. 50, 4303–4334 (2012). doi:10.1016/j.carbon.2012.05.017
24. Guo, Y.-B., Zhang, S.-W.: The Tribological Properties of Multi-Layered Graphene as Additives of PAO2 Oil in Steel–Steel Contacts. Lubricants. 4, 30 (2016). doi:10.3390/lubricants4030030
25. Bagi, S., Vyavhare, K., Aswath, P.B.: Tribological characteristics of greases with and without metallo-organic friction-modifiers. Tribol. - Mater. Surfaces Interfaces. 12, 223–236 (2018). doi:10.1080/17515831.2018.1542790
26. Khare, H.S., Lahouij, I., Jackson, A., Feng, G., Chen, Z., Cooper, G.D., Carpick, R.W.: Nanoscale Generation of Robust Solid Films from Liquid-Dispersed Nanoparticles via in Situ Atomic Force Microscopy: Growth Kinetics and Nanomechanical Properties. ACS Appl. Mater. Interfaces. 10, 40335–40347 (2018). doi:10.1021/acsami.8b16680
27. Battez], A. [Hernández, Viesca, J.L., González, R., Blanco, D., Asedegbega, E., Osorio, A.: Friction reduction properties of a CuO nanolubricant used as lubricant for a NiCrBSi coating. Wear. 268, 325–328 (2010). doi:https://doi.org/10.1016/j.wear.2009.08.018
28. Tao, X., Jiazheng, Z., Kang, X.: The ball-bearing effect of diamond nanoparticles as an oil additive. J. Phys. D. Appl. Phys. 29, 2932–2937 (1996). doi:10.1088/0022-3727/29/11/029
29. Chou, C.-C., Lee, S.-H.: Tribological behavior of nanodiamond-dispersed lubricants on carbon steels and aluminum alloy. Wear. 269, 757–762 (2010). doi:https://doi.org/10.1016/j.wear.2010.08.001
30. Dou, X., Koltonow, A.R., He, X., Jang, H.D., Wang, Q., Chung, Y.-W., Huang, J.: Self-dispersed crumpled graphene balls in oil for friction and wear reduction. Proc. Natl. Acad. Sci. (2016). doi:10.1073/pnas.1520994113

31. Lee, J., Cho, S., Hwang, Y., Lee, C., Kim, S.H.: Enhancement of Lubrication Properties of Nano-oil by Controlling the Amount of Fullerene Nanoparticle Additives. Tribol. Lett. 28, 203–208 (2007). doi:10.1007/s11249-007-9265-2
32. Vyavhare, K., Aswath, P.B.: Tribological Properties of Novel Multi-Walled Carbon Nanotubes and Phosphorus Containing Ionic Liquid Hybrids in Grease. Front. Mech. Eng. 5, 15 (2019). doi:10.3389/fmech.2019.00015
33. Machado, A.H.E., Lundberg, D., Ribeiro, A.J., Veiga, F.J., Lindman, B., Miguel, M.G., Olsson, U.: Preparation of Calcium Alginate Nanoparticles Using Water-in-Oil (W/O) Nanoemulsions. Langmuir. 28, 4131–4141 (2012). doi:10.1021/la204944j
34. Zhang, M., Wang, X., Fu, X., Xia, Y.: Performance and anti-wear mechanism of CaCO3 nanoparticles as a green additive in poly-alpha-olefin. Tribol. Int. 42, 1029–1039 (2009). doi:https://doi.org/10.1016/j.triboint.2009.02.012
35. Jiusheng, L., Lifeng, H., Xiaohong, X., Tianhui, R.: Tribological synergism of surface-modified calcium borate nanoparticles and sulfurized olefin. Ind. Lubr. Tribol. 64, 217–223 (2012). doi:10.1108/00368791211232762
36. Gupta, R.N., Harsha, A.P.: Synthesis, Characterization, and Tribological Studies of Calcium–Copper–Titanate Nanoparticles as a Biolubricant Additive. J. Tribol. 139, (2016). doi:10.1115/1.4033714
37. Sánchez-López, J.C., Abad, M.D., Kolodziejczyk, L., Guerrero, E., Fernández, A.: Surface-modified Pd and Au nanoparticles for anti-wear applications. Tribol. Int. 44, 720–726 (2011). doi:https://doi.org/10.1016/j.triboint.2009.12.013
38. Kolodziejczyk, L., Martinez-Martinez, D., Rojas, T. C., Fernández, A., Sánchez-López, J. C.: Surface-modified Pd nanoparticles as a superior additive for lubrication. J. Nanoparticle Res. 9, 639–645 (2007). doi:10.1007/s11051-006-9124-3
39. Viesca, J.L., Hernández Battez, A., González, R., Chou, R., Cabello, J.J.: Antiwear properties of carbon-coated copper nanoparticles used as an additive to a polyalphaolefin. Tribol. Int. 44, 829–833 (2011). doi:https://doi.org/10.1016/j.triboint.2011.02.006
40. Sunqing, Q., Zhou, Z., Junxiu, D., Chen, G.: Preparation of Ni Nanoparticles and Evaluation of Their Tribological Performance as Potential Additives in Oils . J. Tribol. 123, 441–443 (1999). doi:10.1115/1.1286152
41. Cho, J., Denes, F.S., Timmons, R.B.: Plasma Processing Approach to Molecular Surface Tailoring of Nanoparticles: Improved Photocatalytic Activity of TiO2. Chem. Mater. 18, 2989–2996 (2006). doi:10.1021/cm060212g
42. Sumitsawan, S., Cho, J., Sattler, M.L., Timmons, R.B.: Plasma Surface Modified TiO2 Nanoparticles: Improved Photocatalytic Oxidation of Gaseous m-Xylene. Environ. Sci. Technol. 45, 6970–6977 (2011). doi:10.1021/es2012963
43. Savage, C.R., Timmons, R.B., Lin, J.W.: Molecular Control of Surface Film Compositions via Pulsed Radio-Frequency Plasma Deposition of Perfluoropropylene Oxide. 575–577 (1991). doi:10.1021/cm00016a005

44. Hamrock, B.J., Dowson, D.: Isothermal Elastohydrodynamic Lubrication of Point Contacts: Part III—Fully Flooded Results. J. Lubr. Technol. 99, 264–275 (1977). doi:10.1115/1.3453074
45. Yamaguchi, E.S., Ryason, P.R., Hansen, T.P.: Electrical contact resistance studies on zinc dithiophosphates. Tribol. Lett. 3, 27–33 (1997). doi:10.1023/A:1019175509680
46. So, H., Lin, Y.C., Huang, G.G.S., Chang, T.S.T.: Antiwear mechanism of zinc dialkyl dithiophosphates added to a paraffinic oil in the boundary lubrication condition. Wear. 166, 17–26 (1993). doi:https://doi.org/10.1016/0043-1648(93)90274-P
47. Topolovec-Miklozic, K., Forbus, T.R., Spikes, H.A.: Film thickness and roughness of ZDDP antiwear films. Tribol. Lett. 26, 161–171 (2007). doi:10.1007/s11249-006-9189-2
48. Spikes, H.A.: The History and Mechanisms of ZDDP. Tribol. Lett. 17, 469–489 (2004). doi:10.1023/B:TRIL.0000044495.26882.b5
49. Dawczyk, J., Morgan, N., Russo, J., Spikes, H.: Film Thickness and Friction of ZDDP Tribofilms. Tribol. Lett. 67, 34 (2019). doi:10.1007/s11249-019-1148-9
50. Li, Y.-R., Pereira, G., Lachenwitzer, A., Kasrai, M., Norton, P.R.: X-Ray Absorption Spectroscopy and Morphology Study on Antiwear Films Derived from ZDDP Under Different Sliding Frequencies. Tribol. Lett. 27, 245–253 (2007). doi:10.1007/s11249-007-9213-1
51. Morina, A., Green, J.H., Neville, A., Priest, M.: Surface and Tribological Characteristics of Tribofilms Formed in the Boundary Lubrication Regime with Application to Internal Combustion Engines. Tribol. Lett. 15, 443–452 (2003). doi:10.1023/B:TRIL.0000003065.37526.84
52. Najman, M.N., Kasrai, M., Bancroft, G.M.: X-ray Absorption Spectroscopy and Atomic Force Microscopy of Films Generated from Organosulfur Extreme-Pressure (EP) Oil Additives. Tribol. Lett. 14, 225–235 (2003). doi:10.1023/A:1022650516272
53. Hesse, B., Salome, M., Castillo-Michel, H., Cotte, M., Fayard, B., Sahle, C.J., De Nolf, W., Hradilova, J., Masic, A., Kanngießer, B., Bohner, M., Varga, P., Raum, K., Schrof, S.: Full-Field Calcium K-Edge X-ray Absorption Near-Edge Structure Spectroscopy on Cortical Bone at the Micron-Scale: Polarization Effects Reveal Mineral Orientation. Anal. Chem. 88, 3826–3835 (2016). doi:10.1021/acs.analchem.5b04898
54. Cebe, T., Ahuja, N., Monte, F., Awad, K., Vyavhare, K., Aswath, P., Huang, J., Brotto, M., Varanasi, V.: Novel 3D-printed methacrylated chitosan-laponite nanosilicate composite scaffolds enhance cell growth and biomineral formation in MC3T3 pre-osteoblasts. J. Mater. Res. 35, 58–75 (2020). doi:DOI: 10.1557/jmr.2018.260
55. Varlot, K., Kasrai, M., Bancroft, G.M., Yamaguchi, E.S., Ryason, P.R., Igarashi, J.: X-ray absorption study of antiwear films generated from ZDDP and borate micelles. Wear. 249, 1029–1035 (2001). doi:10.1016/S0043-1648(01)00586-5
56. Zhang, Y., Zeng, X., Wu, H., Li, Z., Ren, T., Zhao, Y.: The Tribological Chemistry of a Novel Borate Ester Additive and Its Interaction with ZDDP Using XANES and XPS. Tribol. Lett. 53, 533–542 (2014). doi:10.1007/s11249-013-0292-x

57. Zhang, Z., Yamaguchi, E.S., Kasrai, M., Bancroft, G.M.: Interaction of ZDDP with Borated Dispersant Using XANES and XPS. Tribol. Trans. 47, 527–536 (2004). doi:10.1080/05698190490500725
58. Fofanov, D.: Synthesis, characterization and physical properties of metal borides, http://ediss.sub.uni-hamburg.de/volltexte/2009/2995, (2006)
59. Fleet, M.E., Muthupari, S.: Coordination of boron in alkali borosilicate glasses using XANES. J. Non. Cryst. Solids. 255, 233–241 (1999). doi:10.1016/S0022-3093(99)00386-5
60. Fleet, M.E., Muthupari, S.: Boron K-edge XANES of borate and borosilicate minerals. Am. Mineral. 85, 1009–1021 (2000). doi:10.2138/am-2000-0716
61. Zhang, Z., Yamaguchi, E.S., Kasrai, M., Bancroft, G.M.: Interaction of ZDDP with borated dispersant using XANES and XPS. Tribol. Trans. 47, 527–536 (2004). doi:10.1080/05698190490500725
62. Sharma, V., Timmons, R., Erdemir, A., Aswath, P.B.: Plasma-Functionalized Polytetrafluoroethylene Nanoparticles for Improved Wear in Lubricated Contact. ACS Appl. Mater. Interfaces. 9, 25631–25641 (2017). doi:10.1021/acsami.7b06453
63. Yin, Z., Kasrai, M., Bancroft, G.M., Laycock, K.F., Tan, K.H.: Chemical characterization of antiwear films generated on steel by zinc dialkyl dithiophosphate using X-ray absorption spectroscopy. Tribol. Int. 26, 383–388 (1993). doi:https://doi.org/10.1016/0301-679X(93)90076-D
64. Vyavhare, K., Bagi, S., Patel, M., Aswath, P.B.: Impact of Diesel Engine Oil Additives–Soot Interactions on Physiochemical, Oxidation, and Wear Characteristics of Soot. Energy & Fuels. 33, 4515–4530 (2019). doi:10.1021/acs.energyfuels.8b03841
65. Yin, Z., Kasrai, M., Fuller, M., Bancroft, G.M., Fyfe, K., Tan, K.H.: Application of soft X-ray absorption spectroscopy in chemical characterization of antiwear films generated by ZDDP Part I: the effects of physical parameters. Wear. 202, 172–191 (1997). doi:https://doi.org/10.1016/S0043-1648(96)07272-9
66. Fuller, M., Yin, Z., Kasrai, M., Bancroft, G.M., Yamaguchi, E.S., Ryason, P.R., Willermet, P.A., Tan, K.H.: Chemical characterization of tribochemical and thermal films generated from neutral and basic ZDDPs using X-ray absorption spectroscopy. Tribol. Int. 30, 305–315 (1997). doi:10.1016/S0301-679X(96)00059-X
67. Nicholls, M., Najman, M., Zhang, Z., Kasrai, M., Norton, P., Gilbert, P.: The contribution of XANES spectroscopy to tribology. Can. J. Chem. 85, 816–830 (2007). doi:10.1139/V07-093
68. Najman, M.N., Kasrai, M., Bancroft, G.M., Frazer, B.H., Stasio, G. De: The Correlation of Microchemical Properties to Antiwear (AW) Performance in Ashless Thiophosphate Oil Additives. Tribol. Lett. 17, 811–822 (2004). doi:10.1007/s11249-004-8089-6
69. Yang, S., Wang, D., Liang, G., Yiu, Y.M., Wang, J., Liu, L., Sun, X., Sham, T.-K.: Soft X-ray XANES studies of various phases related to LiFePO4 based cathode materials. Energy Environ. Sci. 5, 7007–7016 (2012). doi:10.1039/C2EE03445J
70. Spikes, H.: The history and mechanisms of ZDDP. Tribol. Lett. 17, 469–489 (2004). doi:10.1023/B:TRIL.0000044495.26882.b5

71. Najman, M.N., Kasrai, M., Bancroft, G.M.: Chemistry of Antiwear Films from Ashless Thiophosphate Oil Additives. Tribol. Lett. 17, 217–229 (2004). doi:10.1023/B:TRIL.0000032448.77085.f4
72. Kim, B., Mourhatch, R., Aswath, P.B.: Properties of tribofilms formed with ashless dithiophosphate and zinc dialkyl dithiophosphate under extreme pressure conditions. Wear. 268, 579–591 (2010). doi:10.1016/j.wear.2009.10.004
73. Najman, M., Kasrai, M., Michael Bancroft, G., Davidson, R.: Combination of ashless antiwear additives with metallic detergents: interactions with neutral and overbased calcium sulfonates. Tribol. Int. 39, 342–355 (2006). doi:10.1016/j.triboint.2005.02.014
74. Mosey, N.J., Müser, M.H., Woo, T.K.: Molecular Mechanisms for the Functionality of Lubricant Additives. Science (80-.). 307, 1612–1615 (2005). doi:10.1126/science.1107895
75. Ueda, M., Kadiric, A., Spikes, H.: On the Crystallinity and Durability of ZDDP Tribofilm. Tribol. Lett. 67, 123 (2019). doi:10.1007/s11249-019-1236-x

Figures

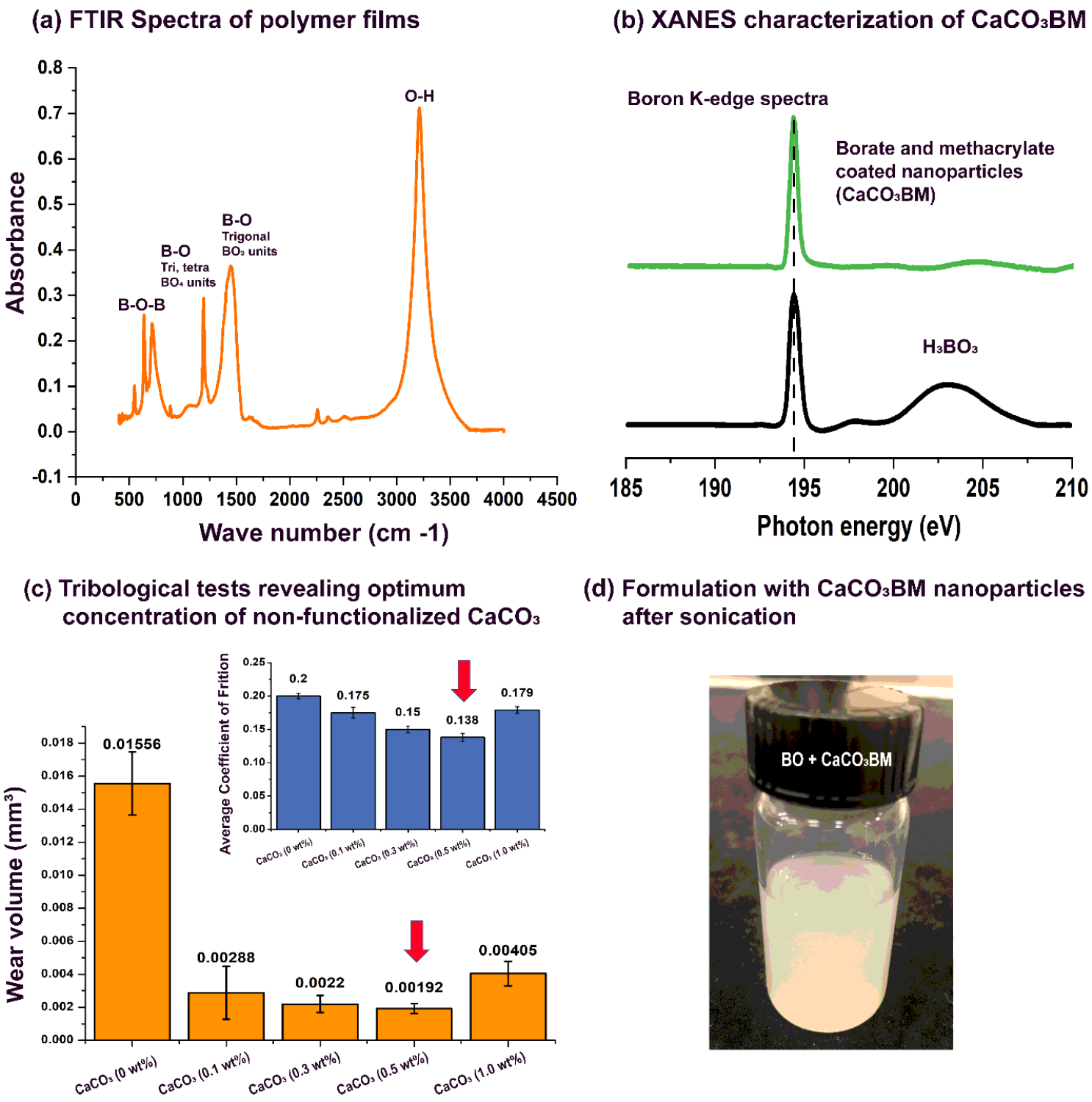

Figure 1

(a) FTIR characterization of plasma polymer films generated with trimethyl boroxine monomer; (b) XANES characterization of plasma functionalized nanoparticles; (c) Preliminary tribological test results with non-functionalized CaCO3 nanoparticles indicating an optimum concentration of 0.5 wt.%; (d) Image of functionalized CaCO3BM nanoparticles uniformly dispersed in the mineral base oil after probe sonication

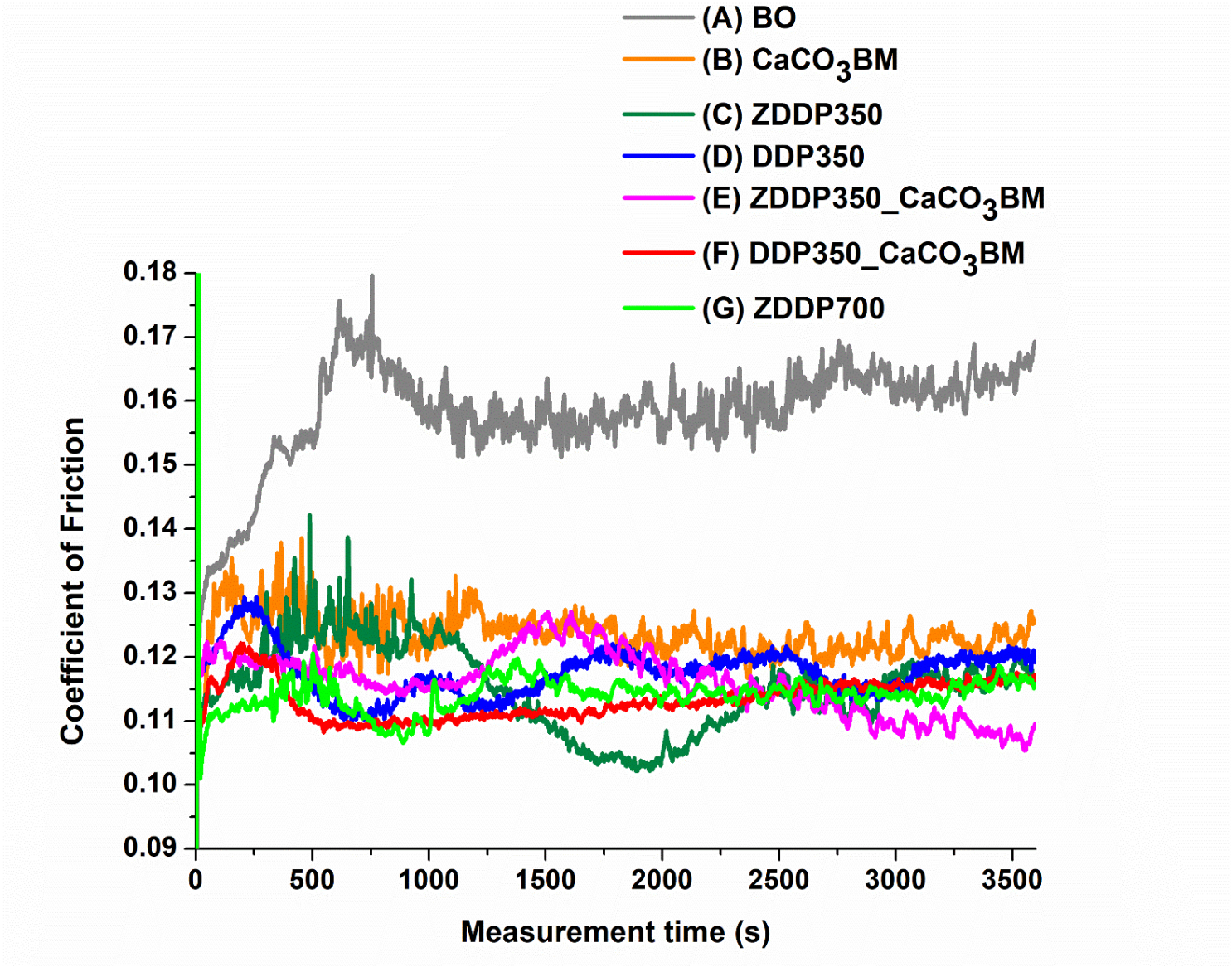

Figure 2

Friction results for samples BO, CaCO3BM, ZDDP350, DDP350, ZDDP350_CaCO3BM, DDP_CaCO3BM, and ZDDP700

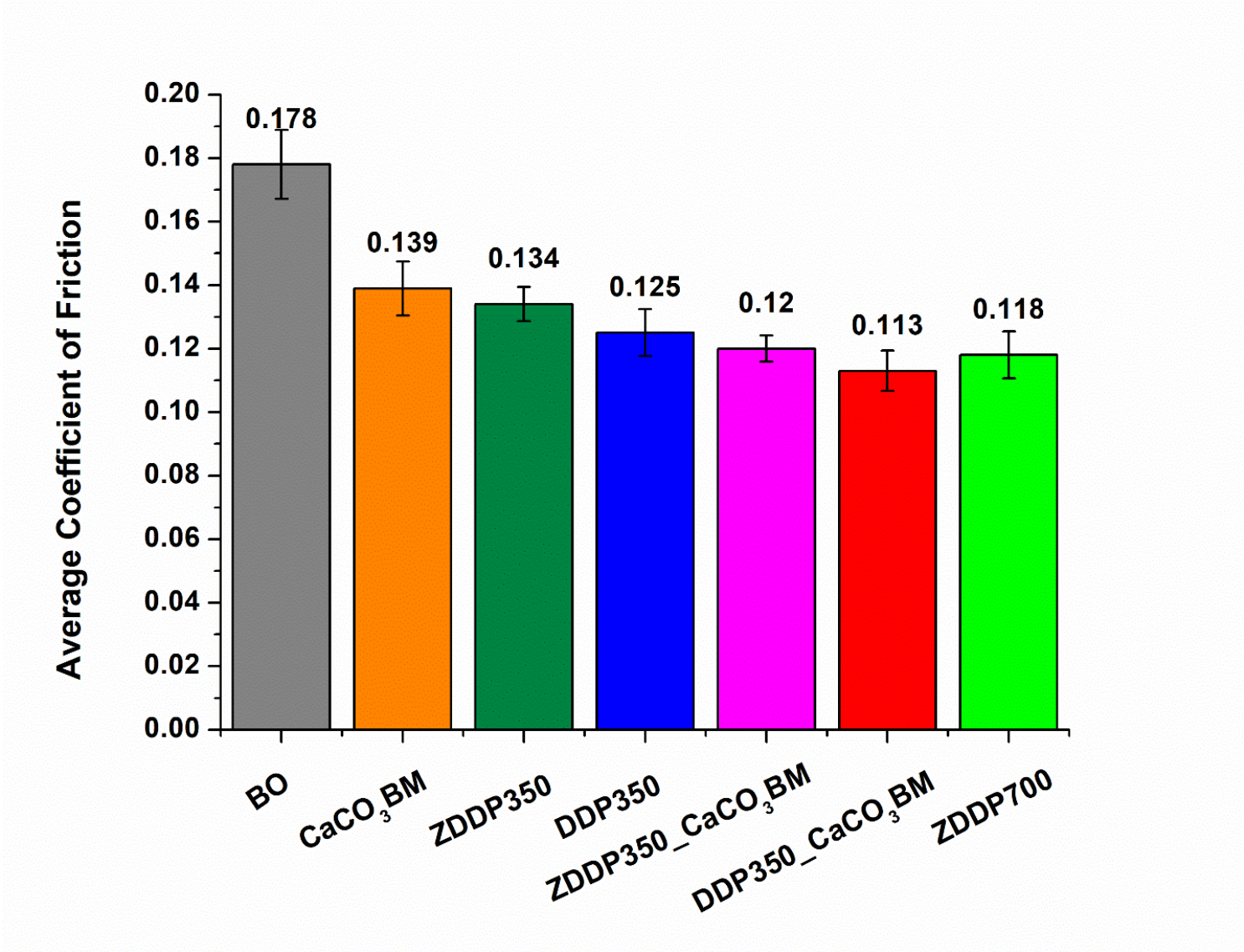

Figure 3

Average coefficient of friction calculated for 60 min duration tribological tests for all oil formulations

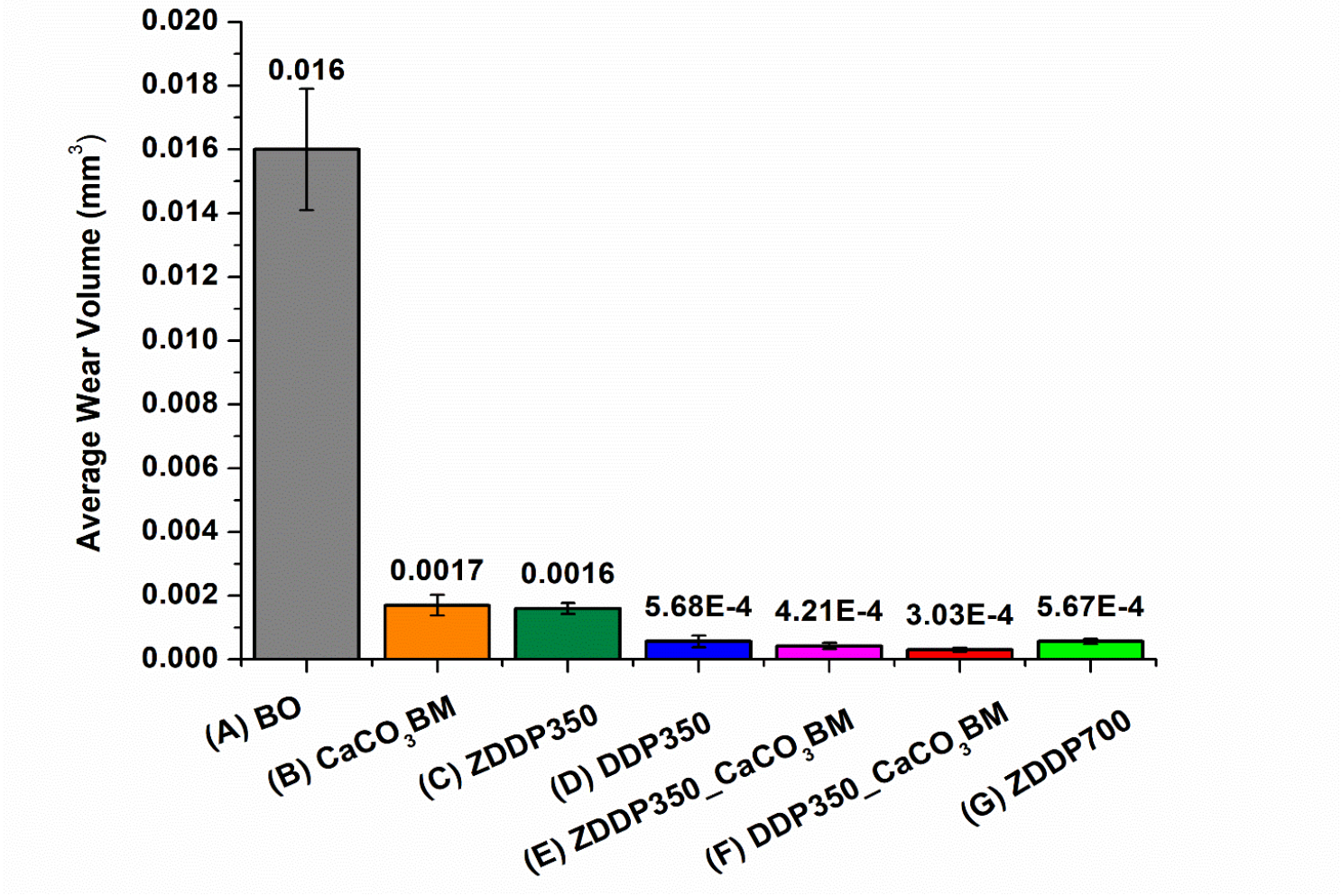

Figure 4

Wear volume results for samples (A) BO (B) CaCO3BM (C) ZDDP350 (D) DDP350 (E) ZDDP350_CaCO3BM (F) DDP350_CaCO3BM and (G) ZDDP700

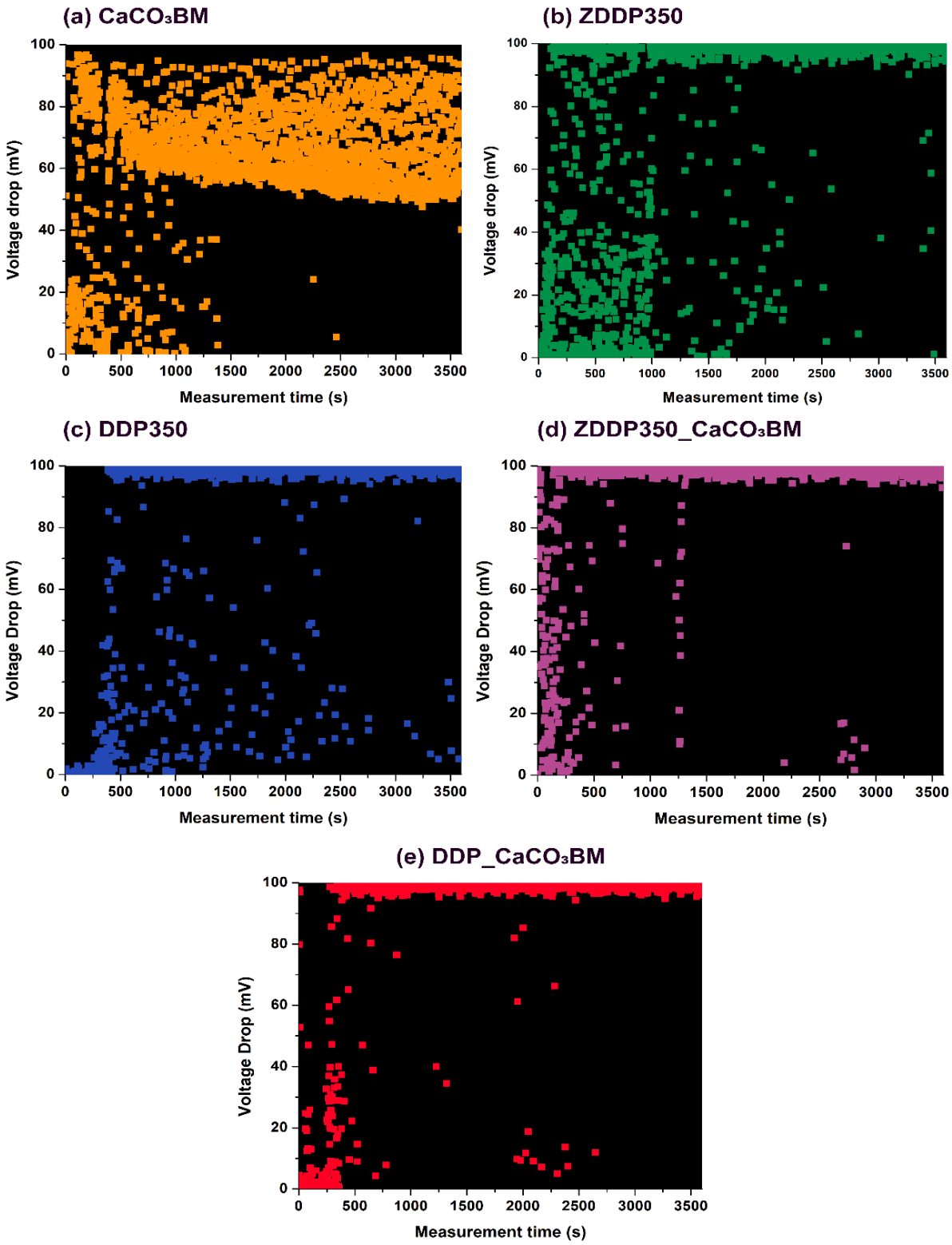

Figure 5

Electrical contact resistance data plotted as the function of test time for formulations (a) BO; (b) CaCO3BM; (c) ZDDP350; (d) DDP350; (e) ZDDP350_CaCO3BM; (f) DDP350_CaCO3BM

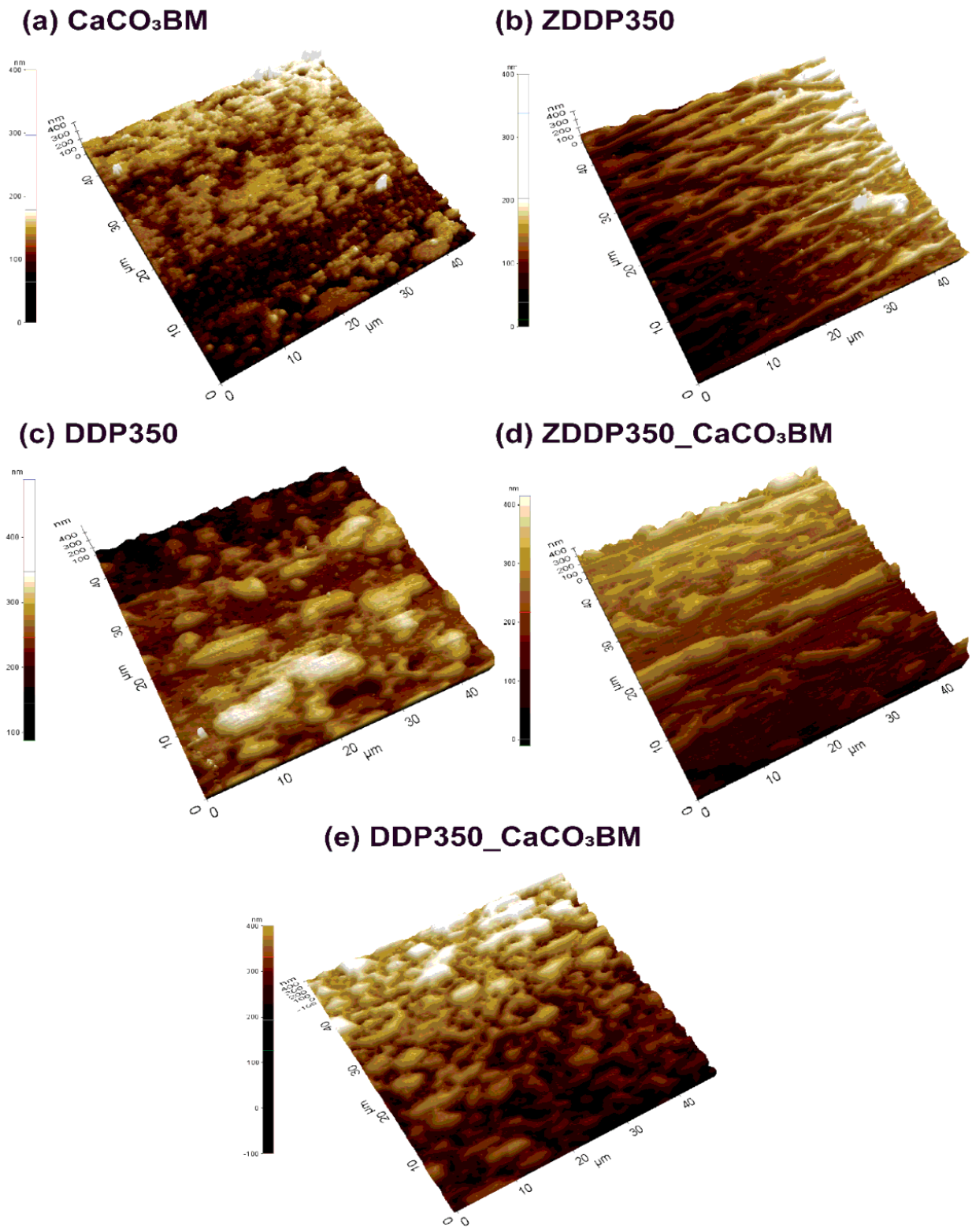

Figure 6

AFM topographical images of the wear scar generated on the flat steel specimen for formulations (a) CaCO3BM; (b) ZDDP350; (c) DDP350; (d) ZDDP350_CaCO3BM; (e) DDP350_CaCO3BM

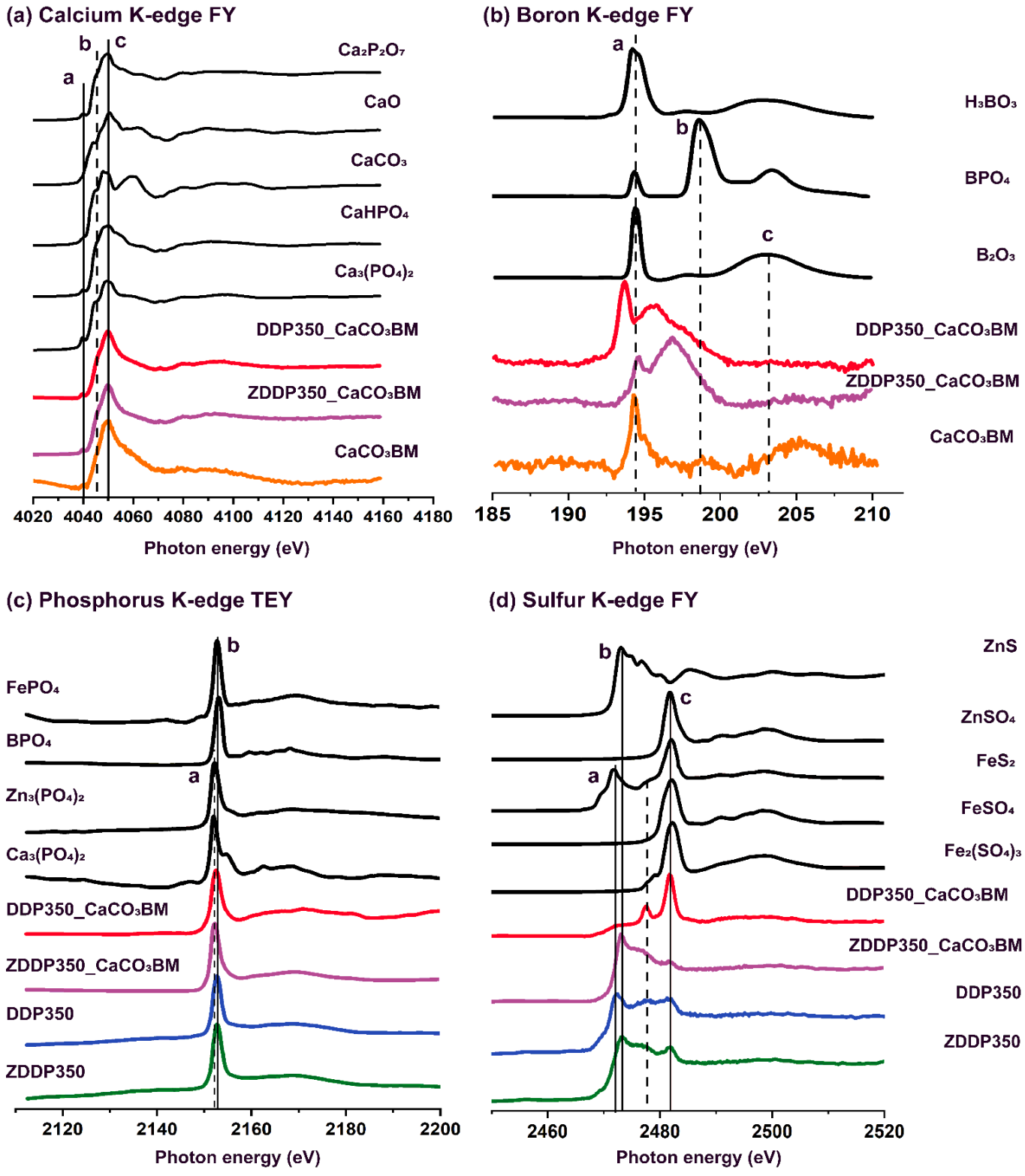

Figure 7

XANES K-edge characterization of tribofilms formed by all prepared oil formulations detailing information on (A) Calcium K-edge TEY; (b) Boron K-edge FY; (c) Phosphorus K-edge TEY; (d) Sulfur K-edge FY

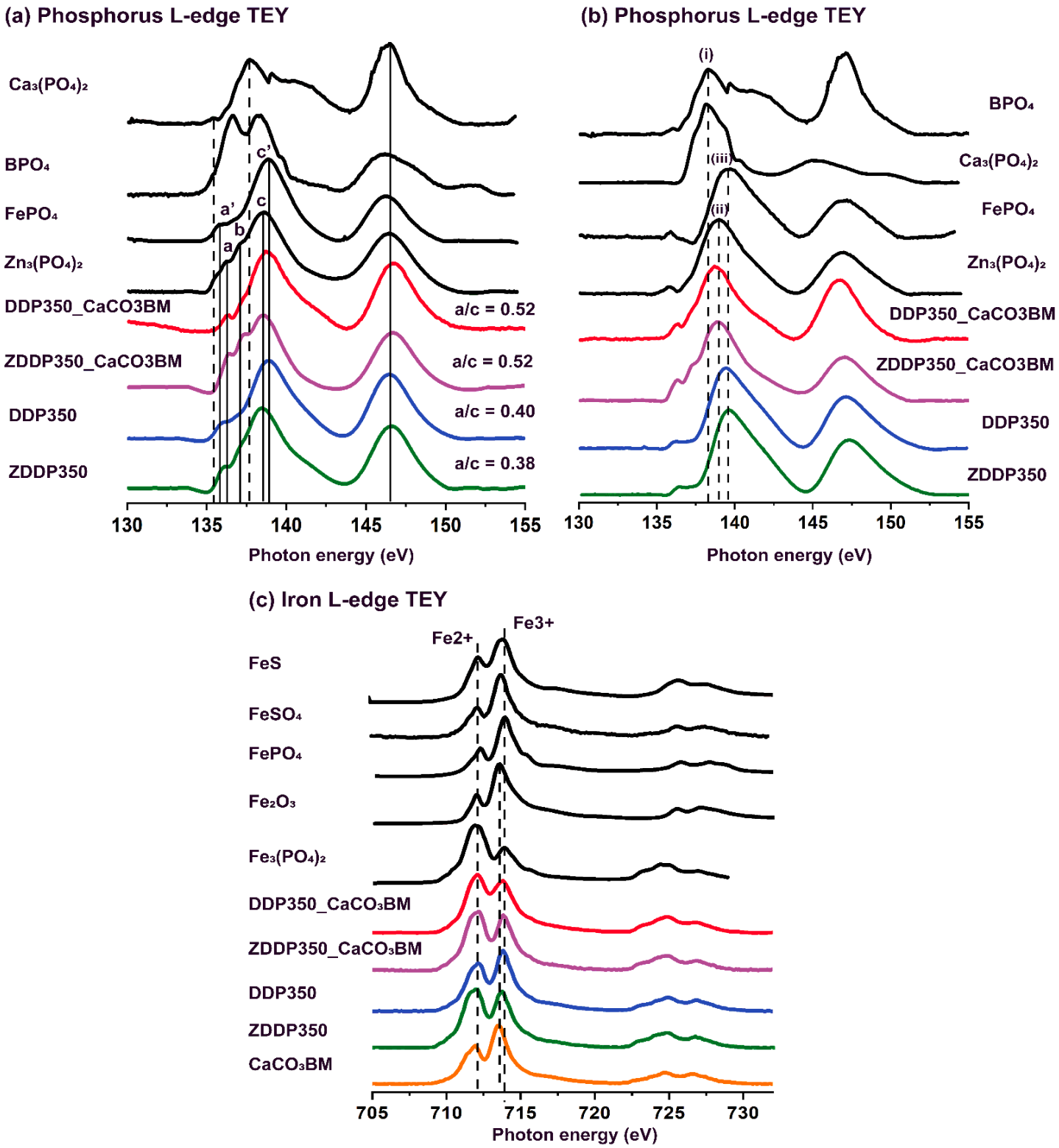

Figure 8

XANES L-edge characterization of tribofilms formed by all prepared oil formulations detailing information on (a) Phosphorus L-edge TEY; (b) Phosphorus L-edge FY; (c) Iron L-edge TEY

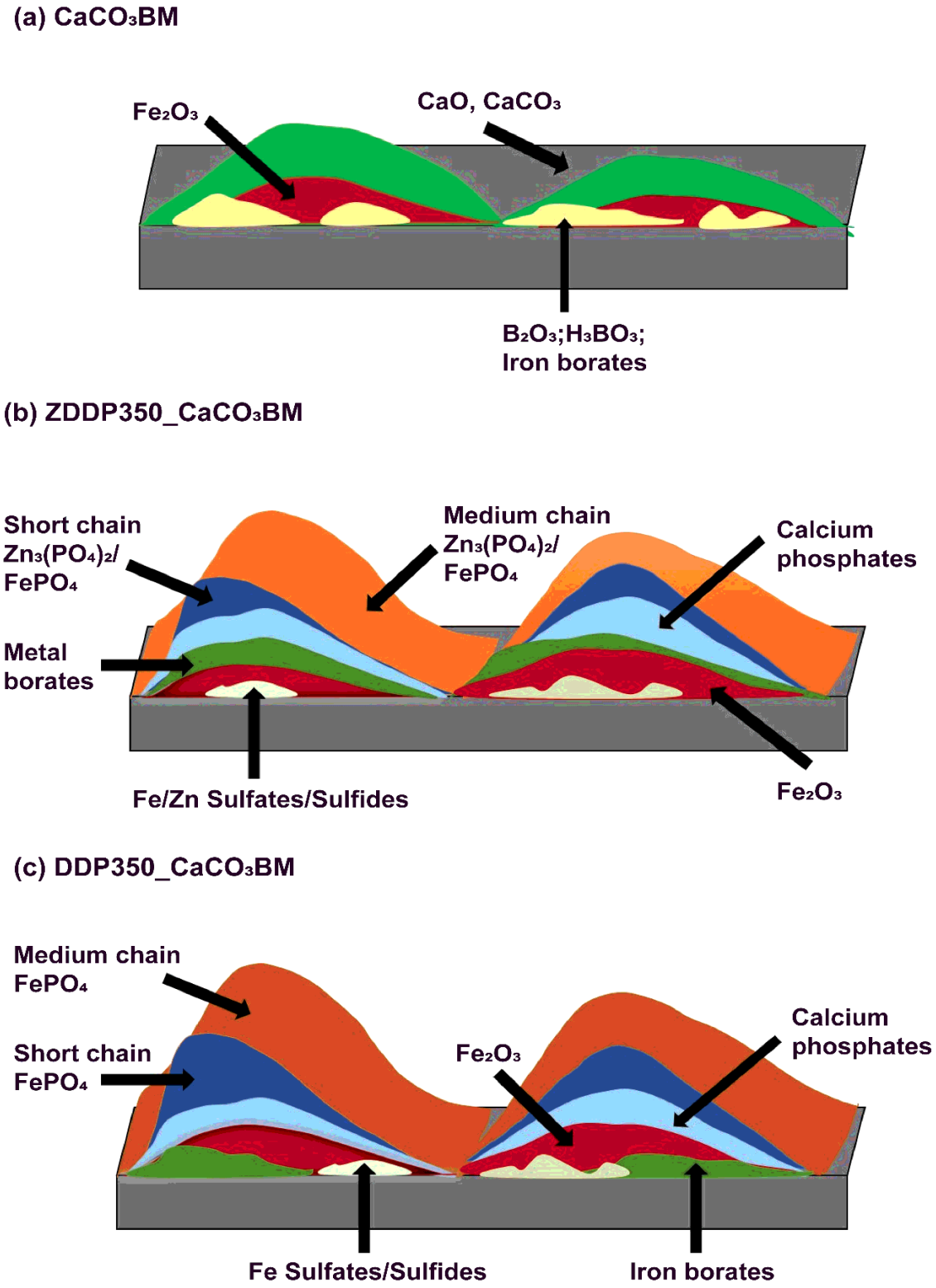

Figure 9

Tribofilm models created from the XANES and AFM results for samples (a) CaCO3BM; (b) ZDDP350_ CaCO3BM; and (c) DDP350_ CaCO3BM

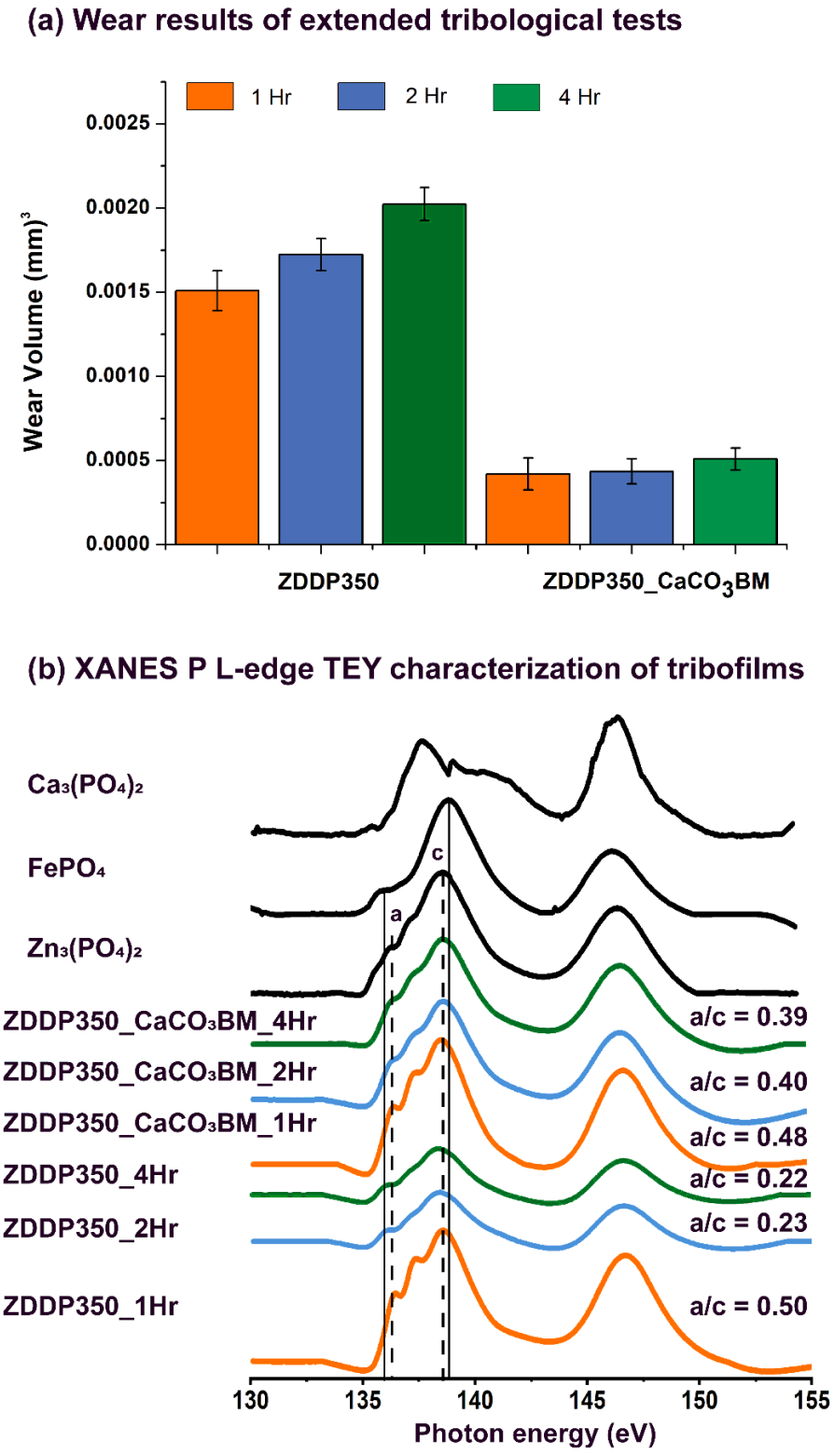

Figure 10

(a) Tribological test wear results for rubbing duration of 1 Hr, 2 Hr, and 4 Hr; (b) XANES P L-edge TEY spectra exhibiting a change in phosphate chain length with rubbing time

Supplementary Files

This is a list of supplementary files associated with this preprint. Click to download.

- SupportingInformation.docx